relaxant. We observed the same EP component, but for the first time identified the early component, which did not disappear under muscle relaxation. The early component P1–N1 complex shifted earlier when the stimulation electrodes were moved rostrally. It was specific to vagal stimulation because stimulation of the ansa cervicalis, very close to the VN, did not induce any EP. Therefore, it was highly probable that the P1–N1 we observed was direct evidence of the afferent conduction of the VN in humans.

The reason why previous researchers were unable to recognize the early EP component is unclear [12,13]. But they seemed to focus on long-latency potentials from the outset of their studies. As we demonstrated here, the early component was easily buried in the initial stimulation wave. To detect the early component constantly, stimulation with shorter pulse widths was preferable. Larger currents and larger pulse widths made the P1–N1 complex less discernable due to the larger initial stimulation wave.

As for the origin of the early component, we observed the largest waveform from the auricle and the mastoid process. Therefore, it was considered to originate from around the brainstem, skullbase, or the upper cervical region. We can estimate the distance between the stimulation point and the generator of EP by multiplying the calculated value of NCV (27 m/s) by the measured value of the N1 latency (3.3 ms). It is estimated to be 89.1 mm, consistent with the distance between the surgical wound in the neck and the skullbase.

The main sources of EPs are axonal-conducting action potentials and postsynaptic potentials. A junctional potential is generated by a change in the size or impedance of the volume conductor around the nerve, by a directional change of the nerve course, or at the beginning or end of the nerve conduction [14]. The VN passes through the jugular foramen and connects to multiple nuclei, including the spinal tract nucleus, the medial reticular formation of the medulla, the area postrema, the dorsal nucleus of the VN, the ambiguous nucleus, and the solitary tract nucleus [15]. Applying the above-mentioned rule to the VN, we can speculate that the early component was most likely generated at the entrance into the cranium, the jugular foramen, where the impedance around the nerve changes. Contributions of the terminal potentials and post-synaptic potentials in the medulla oblongata are considered less likely since the VN disperses to multiple nuclei within it. The above theory of junctional potential may also explain why the N1′ potential recorded in the A2–Cz lead had an earlier peak than the N1 recorded in the A1–Cz lead. Viewing from the A2 electrode position, the ascending impulse along the VN hides itself behind the massive cranial bone and vertebra, before its true entrance into the

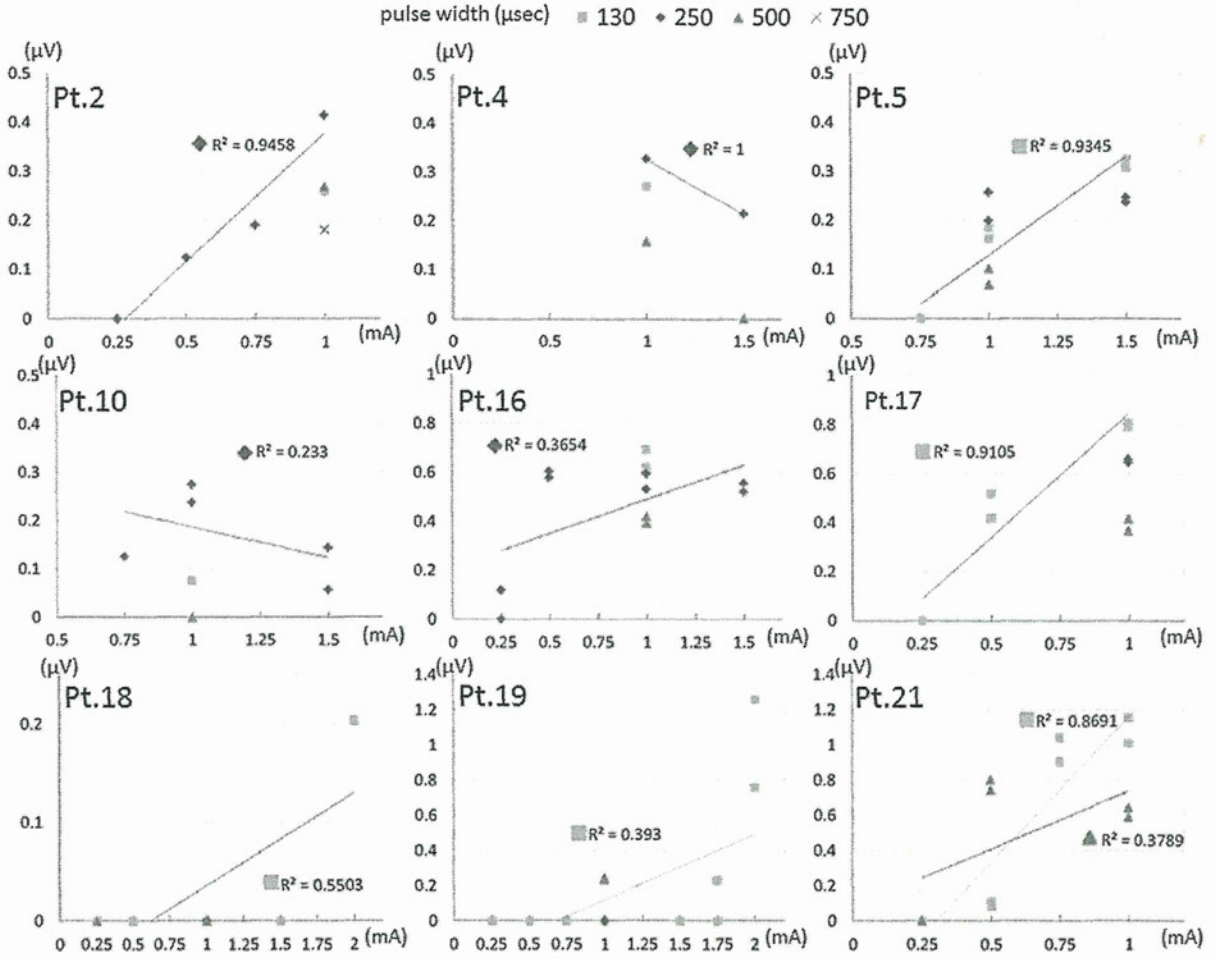

Figure 7. Association between the amplitude of P1–N1 complex and the VNS parameters in 9 patients. Horizontal and vertical axes represent the current and the estimated amplitude of the P1–N1 complex, respectively. For estimation of the amplitude of the P1–N1 complex, see the 'Data analysis' section of the text. Each regression line represents the association of current and amplitude to a fixed value of pulse width. R^2 is the correlation coefficient. In Patient 21, two regression lines are shown because we recorded with multiple currents to pulse widths of 130 μs (—) and 500 μs (—). In 7 of 9 patients, an increase in stimulation current resulted in an associated increase in the amplitude, while the pulse width did not affect the amplitude.

skullbase. Therefore, the junctional potential may be generated slightly earlier than the N1 potential.

As for the late component, we postulated that the P2–N2 complex was the same potential as that observed in a previous study [12]. It is highly probable that the P2–N2 complex reflects the laryngopharyngeal electromyogram, since it disappeared after the administration of a muscle relaxant and its waveform was similar to that in endotracheal electrodes. The finding that their latencies were slightly later than those in the laryngopharyngeal electrodes and that their waveforms were almost symmetrical in A1–Cz and A2–Cz suggests that the generator was located far away and in the center, supporting the laryngopharyngeal electromyogram notion.

Eighty percent of the VN at the cervical portion is afferent fiber [16], which consists of 3 components, Aβ, Aγ and C fibers [17,18]. The conduction velocity of Aβ fibers is the fastest and that of C fibers is the slowest. The threshold producing an action potential is the lowest in Aβ fibers and the highest in C fibers. Previous studies suggested that the neural conduction of A fibers contributes to antiepileptic effects [9,18,19]. The estimated nerve conduction velocity was 27.4 ± 10.2 m/s in our study, which fell in the range of A fibers and was consistent with previous studies.

This study was the first to demonstrate in a clinical setting that VNS in humans generates ascending afferent nerve conduction, revealing some aspects of electrophysiological properties of the human VN. We did not directly prove the clinical usefulness for the recording of VN-EP, but we assume its significance in two aspects: First, it can be used to confirm the VN intraoperatively; in some patients, the ansa cervicalis is very thick and for inexperienced surgeons there may be a risk of misjudgment, particularly when the implantation surgery is done with a very small surgical wound. Second, the recording of VN-EP may explain the cause of treatment failure in some patients and might predict the outcome of treatment. For that purpose, further research is needed to study the association of VN-EP properties and the efficacy of VNS in epilepsy patients.

Acknowledgments

The authors thank Mr. Hitoshi Sano of Nihon Kohden Corporation for his technical and theoretical support.

Supplementary data

Supplementary data related to this article can be found online at http://dx.doi.org/10.1016/j.brs.2012.09.007

References

[1] Ben-Menachem E. Vagus-nerve stimulation for the treatment of epilepsy. Lancet Neurology 2002;1(8):477–82.
[2] Clark KB, Naritoku DK, Smith DC, Browning RA, Jensen RA. Enhanced recognition memory following vagus nerve stimulation in human subjects. Nature Neuroscience 1999;2(1):94–8.
[3] Elger G, Hoppe C, Falkai P, Rush AJ, Elger CE. Vagus nerve stimulation is associated with mood improvements in epilepsy patients. Epilepsy Research 2000;42(2-3):203–10.
[4] Naritoku DK, Terry WJ, Helfert RH. Regional induction of fos immunoreactivity in the brain by anticonvulsant stimulation of the vagus nerve. Epilepsy Research 1995;22(1):53–62.
[5] Walker BR, Easton A, Gale K. Regulation of limbic motor seizures by GABA and glutamate transmission in nucleus tractus solitarius. Epilepsia 1999;40(8): 1051–7.
[6] Krahl SE, Clark KB, Smith DC, Browning RA. Locus coeruleus lesions suppress the seizure-attenuating effects of vagus nerve stimulation. Epilepsia 1998; 39(7):709–14.
[7] Groves DA, Bowman EM, Brown VJ. Recordings from the rat locus coeruleus during acute vagal nerve stimulation in the anaesthetised rat. Neuroscience Letters 2005;379(3):174–9.
[8] Manta S, Dong J, Debonnel G, Blier P. Enhancement of the function of rat serotonin and norepinephrine neurons by sustained vagus nerve stimulation. Journal of Psychiatry & Neuroscience 2009;34(4):272–80.
[9] Zagon A, Kemeny AA. Slow hyperpolarization in cortical neurons: a possible mechanism behind vagus nerve simulation therapy for refractory epilepsy? Epilepsia 2000;41(11):1382–9.
[10] Henry TR, Votaw JR, Pennell PB, Epstein CM, Bakay RA, Faber TL, et al. Acute blood flow changes and efficacy of vagus nerve stimulation in partial epilepsy. Neurology 1999;52(6):1166–73.
[11] Di Lazzaro V, Oliviero A, Pilato F, Saturno E, Dileone M, Meglio M, et al. Effects of vagus nerve stimulation on cortical excitability in epileptic patients. Neurology 2004;62(12):2310–2.
[12] Hammond EJ, Uthman BM, Reid SA, Wilder BJ. Electrophysiologic studies of cervical vagus nerve stimulation in humans: II. Evoked potentials. Epilepsia 1992;33(6):1021–8.
[13] Tougas G, Hudoba P, Fitzpatrick D, Hunt RH, Upton AR. Cerebral-evoked potential responses following direct vagal and esophageal electrical stimulation in humans. American Journal of Physiology 1993;264(3 Pt 1): G486–91.
[14] Sonoo M. How much has been solved regarding SEP generators? Electroencephalography and Clinical Neurophysiology. Supplement 1999;49: 47–51.
[15] Henry TR. Therapeutic mechanisms of vagus nerve stimulation. Neurology 2002;59(6 Suppl. 4):S3–14.
[16] Foley JO, DuBois FS. Quantitative studies of the vagus nerve in the cat. I. The ratio of sensory to motor fibers. Journal of Comparative Neurology 1937;67: 49–67.
[17] Li CL, Mathews G, Bak AF. Action potential of somatic and autonomic nerves. Experimental Neurology 1977;56(3):527–37.
[18] Evans MS, Verma-Ahuja S, Naritoku DK, Espinosa JA. Intraoperative human vagus nerve compound action potentials. Acta Neurologica Scandinavica 2004;110(4):232–8.
[19] Krahl SE, Senanayake SS, Handforth A. Destruction of peripheral C-fibers does not alter subsequent vagus nerve stimulation-induced seizure suppression in rats. Epilepsia 2001;42(5):586–9.

ELSEVIER

Brain & Development xxx (2013) xxx–xxx

BRAIN & DEVELOPMENT
Official Journal of the Japanese Society of Child Neurology

www.elsevier.com/locate/braindev

Original article

Modification of vertical hemispherotomy for refractory epilepsy ☆

Kensuke Kawai [a,*], Michiharu Morino [b], Masaki Iwasaki [c]

[a] *Department of Neurosurgery, The University of Tokyo, Japan*
[b] *Department of Neurosurgery, Tokyo Metropolitan Neurological Hospital, Japan*
[c] *Department of Neurosurgery, Tohoku University, Japan*

Received 12 November 2012; received in revised form 28 December 2012; accepted 30 December 2012

Abstract

Delalande's vertical hemispherotomy is an innovative evolution of hemispherectomy in minimizing brain resection. We report our modification for this surgical procedure. We modified the original procedure in two aspects for the purpose of less brain resection and confirmation of the complete disconnection. Firstly, all procedures were done via an interhemispheric route instead of a transcortical route. Secondly, we set the anterior disconnection plane as the one that connects the anterior end of the choroidal fissure to the anterior end of the foramen of Monro, instead of the former to the subcallosal area. We applied this modified vertical hemispherotomy to 7 cases. Four cases were children with hemimegalencephaly and other 3 were adults with ulegyric hemisphere. Surgical procedure was completed without complication in all cases. There was no case that required CSF shunting. Seizure outcome was Engel's class I in 6 and class IV in 1. Postoperative MRI revealed complete disconnection of the affected hemisphere in all patients. We reported our modification of vertical hemispherotomy. Although these are minor modifications, they further minimized brain resection and may serve for less invasiveness of procedure and improvement in completeness of disconnection and its confirmation during surgery.

Keywords: Epilepsy; Epilepsy surgery; Hemispherectomy; Hemispherotomy

1. Introduction

Hemispherectomy is the most effective surgical treatment for hemispheric epilepsy. Surgical procedure of hemispherectomy has been developed over the past decades. Functional hemispherectomy by Rasmussen was the first to introduce the concept of disconnection of epileptic cortices [1]. Thereafter, several surgeons modified the procedure to further reduce the volume of brain resection by making the disconnection of the white matter tracts as the major procedure instead of resection [2–5]. These modified functional hemispherectomies are called hemispherotomy. While the most procedures of hemispherotomy used a lateral approach to the brain according to Rasmussen's original functional hemispherectomy [3–5], Delalande first proposed a novel hemispherotomy procedure in 1990s [6]. It was innovative in using a vertical approach and achieving the complete disconnection of affected cortices with much less volume of brain resection than the lateral approaches.

One of the authors reviewed the hemispherotomy series at Tokyo Metropolitan Neurological Hospital [7]. In this study, the procedure was reviewed by decomposing into a disconnection of the commissural fibers and a disconnection of the projection fibers, and the elemental surgical procedures were compared in terms of the completeness of disconnection and the occurrence of complication. The major findings were that interhemispheric

☆ Part of this work has been presented at the International Symposium on Surgery for Catastrophic Epilepsy in Infants (ISCE), the Fourteenth Annual Meeting of ISS, Tokyo, February 18-19, 2012.

* Corresponding author. Address: Department of Neurosurgery, Graduate School of Medicine, The University of Tokyo, 7-3-1 Hongo, Bunkyo, Tokyo 113-8655, Japan. Tel.: +81 3 5800 8853; fax: +81 3 5800 8655.
E-mail address: kenkawai-tky@umin.net (K. Kawai).

0387-7604/$ - see front matter © 2013 Published by Elsevier B.V. on behalf of The Japanese Society of Child Neurology.
http://dx.doi.org/10.1016/j.braindev.2012.12.013

Please cite this article in press as: Kawai K et al. Modification of vertical hemispherotomy for refractory epilepsy. Brain Dev (2013), http://dx.doi.org/10.1016/j.braindev.2012.12.013

Table 1
Clinical information of 7 patients.

Patient	Age at onset of seizure	Type of seizure	Frequency of seizure	Preoperative AED[a]	MRIfindings/ etiology	Distribution of epileptiform abnormality in EEG	Others	Preoperative IQ, DQ or neurological state	Age at surgery	Side of surgery	Follow up (years)	Seizure outcome[b]
1	1 day	GCS	Multiple daily	PB(20) VPA(150) MDZ(0.05)	Lt. hemimegalencephaly	Lt. hemispheric	rCBF-SPECT: rt. hemispheric increase	Hypotonic, minimal extremities movement	2 months	Left	9	I
2	5 years	CPS, HC	Weekly	PHT(300) VPA(1200) CBZ(900) CZP(2)	Rt. hemiatrophy, porencephaly/ cerebral palsy	Rt. hemispheric	FDG-PET: rt. hemispheric decrease	VIQ 60 PIQ 47 FIQ 49	40 years	Right	8	I
3	9 years	MS, TS	Monthly	VPA(1200) CBZ(700) CLB(10)	Lt. diffuse ulegyria/ posttraumatic	Lt. hemispheric	FDG-PET: lt. hemispheric decrease	VIQ 54 PIQ so FIQ 40	21 years	Left	7	I
4	1 day	CPS, HC, TS	Multiple daily	PB(32) ZNS(60) CLB(3.2)	Rt. hemimegalencephaly	Bilateral, diffuse	FDG-PET: rt. temporal decrease	Not tested but delay in milestone	4 months	Right	5	I
5	1 day	GCS HC	Multiple daily	PHT(150) CBZ(400) MDZ(0.3)	Lt. hemimegalencephaly	Lt. hemispheric	FDG-PET: lt. hemispheric decrease	Not tested	6 months	Left	4	I
6	1 day	TS	Multiple daily	PB(100) CBZ(160) PHT(115)	Rt. hemimegalencephaly	Bilateral, diffuse	FDG-PET: rt. hemispheric and left frontal decrease	Not tested	7 months	Right	4	IV
7	1 year	CPS	Multiple daily	CBZ(900) VPA(1200)	Lt. hemiatrophy/ postvaccination	Lt. hemispheric	FDG-PET: rt. hemispheric decrease	VIQ 62 PIQ 49 FIQ 51	41 years	Left	0.5	I

AED, antiepileptic drug; CPS, complex partial seizure; GCS, generalized convulsive seizure; HC, hemiconvulsion; lt., left; MDZ, midazolam; MS, myoclonic seizure; PB, phenobarbital; rt., right; so, scale out; TS, tonic seizure; VPA, valproic acid.

[a] Dose is shown in parenthesis (mg). Midazolam was administered intravenous continuously (mg/kg/h).

[b] Engel's classification. Class I means free of disabling seizures since surgery. Class IV means no worthwhile improvement.

Please cite this article in press as: Kawai K et al. Modification of vertical hemispherotomy for refractory epilepsy. Brain Dev (2013), http://dx.doi.org/10.1016/j.braindev.2012.12.013

callosotomy was securer than transventricular callosotomy, and that the less brain resection results in the less complication associated with circulation of the cerebrospinal fluid. Based on these findings, we adopted Delalande's vertical hemispherotomy because it used vertical callosotomy that is similar to interhemispheric callosotomy and resected only a small volume of the brain. We further made minor modifications to the original vertical hemispherotomy by using the interhemispheric callosotomy and further reducing the volume of brain resection, which we present in this report.

2. Methods

2.1. Patients

We adopted the modified hemispherotomy to 7 patients. Four patients underwent surgery by one of the authors (K.K.) at the University of Tokyo Hospital. The other three underwent surgery by the other two authors and K.K as an assistant. Etiology of epilepsy was hemimegalencephaly in 4 patients who underwent surgery at 2, 4, 6 and 7 months old, perinatal injury in a patient who underwent surgery at 40 years old, post-vaccination status epilepticus in a patient who underwent surgery at 41 years old, and posttraumatic ulegyria in a patient who underwent surgery at 21 years old.

2.2. Preoperative evaluation

Indication for hemispherotomy was determined according to the preoperative workup including long-term video electroencephalography (EEG) monitoring, magnetic resonance imaging (MRI), 2-deoxy-2-[^{18}F]fluoro-D-glucose positron emission tomography, and magnetoencephalography. Developmental tests and neuropsychological tests were done in children and adults, respectively. For adult patients, language dominance was determined by Wada test, and residual motor function of the affected hemisphere was evaluated with somatosensory evoked potential and electromyogram evoked by transcranial magnetic simulation (Table 1).

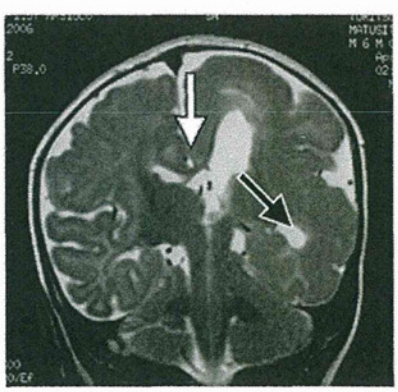

Fig. 1. Schematic image of the modification 1. Callosotomy was performed via an interhemispheric route. Head position, skin incision and craniotomy are the same as callosotomy that is routinely performed as a single surgical procedure. For our modified hemispherotomy, total callosotomy via an interhemispheric approach was first performed (white arrow). Then the lateral border of the thalamus is severed down to the inferior horn of the lateral ventricle (black arrow). When necessary, a small portion of the cingulate gyrus can be resected.

2.3. Surgical technique

We modified the Delalande's original vertical hemispherotomy in two aspects. Firstly, all procedures were done via an interhemispheric route instead of via a transcortical route (Fig. 1). Secondly, we set the anterior disconnection plane as the one that connects the anterior end of the choroidal fissure to the anterior end of the foramen of Monro, instead of the former to the subcallosal area (Fig. 2).

After induction of general anesthesia, patients' head were fixed in a median position with the vertex up. For adult patients, we used a three-point skeletal fixation device. For infants, we fixed their heads on a torus-shaped soft cushion covering them with plastic adhesive wound drapes. We used a U-shaped skin flap. Its anteriormost points were on the frontal hairline and the posteriormost point was a few centimeters behind the bregma. An approximately 7 × 5 cm craniotomy was made over the midline that was larger in the affected side. The dura was opened and reflected medially.

Following procedures were performed under the operative microscope. Firstly, we performed a complete callosotomy according to our routine procedure of callosotomy as a single treatment [8]. In brief, we carefully opened the interhemispheric cistern and exposed the whole length of the superior surface of the body of corpus callosum. The bridging veins were preserved as much as possible. Making the septum pellucidum as a guidance of midline, the corpus callosum was sectioned from the rostrum through the splenium. Then, via the same interhemispheric route, we opened the ependymal roof of the lateral ventricle on the affected side. The foramen of Monro and the choroid plexus that runs posterolaterally from the foramen to the ventricular trigone were visualized with retraction of the lateral wall of the ventricle. The disconnection plane of the projection fibers was the lateral border of the thalamus. Suction and cutting of the lateral border of thalamus was advanced anteriorly from the trigone to the anteriormost point of the choroidal fissure in the inferior horn of lateral ventricle. The choroid plexus in the inferior horn was a nice guidance in this process. Then, we cut the anterior border of the thalamus by connecting the resection from the anteriormost point of the choroidal

Please cite this article in press as: Kawai K et al. Modification of vertical hemispherotomy for refractory epilepsy. Brain Dev (2013), http://dx.doi.org/10.1016/j.braindev.2012.12.013

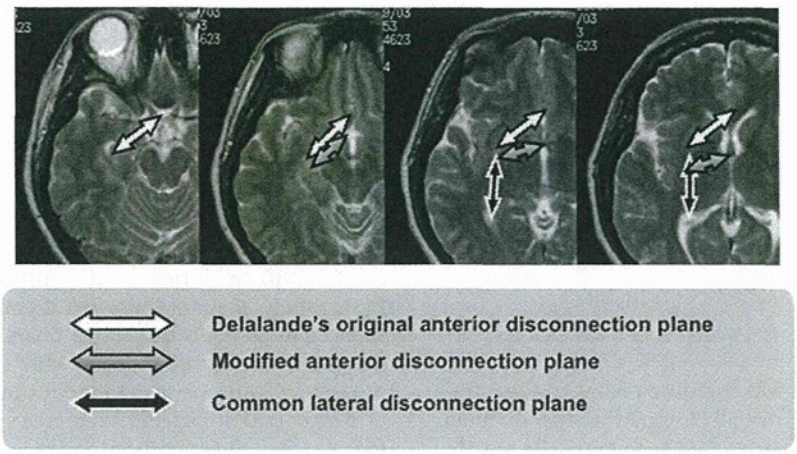

Fig. 2. Schematic image of the modification 2. The anterior disconnection plane as the one that connects the anterior end of the choroidal fissure to the anterior end of the foramen of Monro (gray arrow), instead of the former to the subcallosal area in the Delalande's original method (white arrow). Black arrow is the lateral disconnection plane common to the both methods.

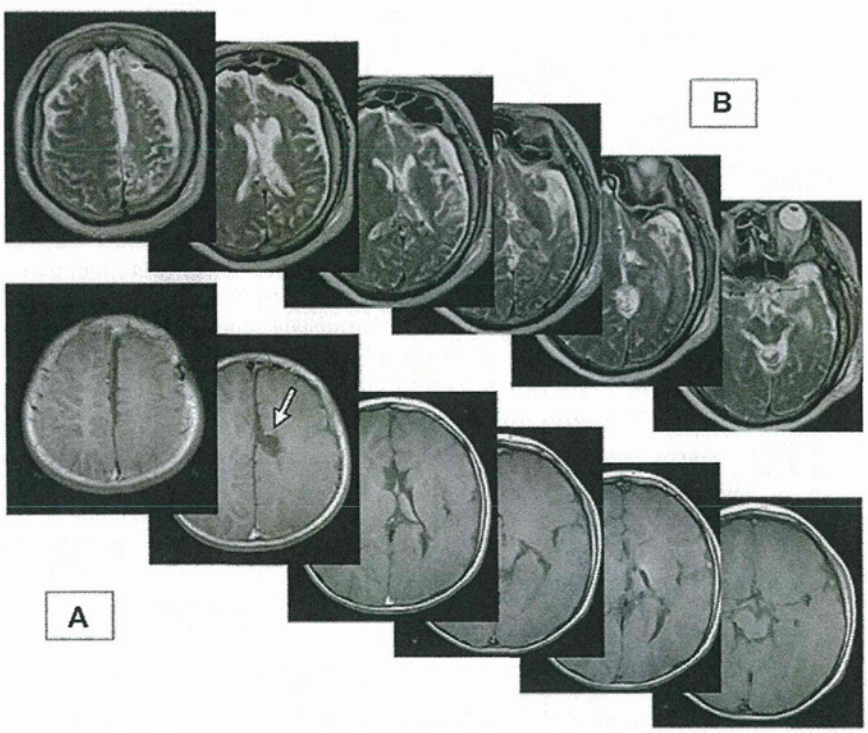

Fig. 3. Serial images of postoperative MRI in the representative patients. (A) Two years after surgery in an infant with hemimegalencephaly. (B) Two days after surgery in an adult with hemiatrophy. In both patients, the corpus callosotomy was completely disconnected via an interhemispheric approach and the thalamus was completely disconnected by the minimal cutting plane. In A, a small part of the cingulate gyrus was resected to gain the lateral view.

fissure to the anteriormost point of the foramen of Monro. Thus disconnection of the projection fibers from the neocortices was completed. Finally, we cut the fornix, the projection fibers of the limbic system, at the ventricular trigone.

The lateral ventricle was rinsed and filled with the artificial cerebrospinal fluid. The roof of the lateral ventricle was closed with a gelatin sponge using fibrin glue. The dura, skull and skin were closed in a usual manner.

Please cite this article in press as: Kawai K et al. Modification of vertical hemispherotomy for refractory epilepsy. Brain Dev (2013), http://dx.doi.org/10.1016/j.braindev.2012.12.013

2.4. Postoperative evaluation

The completeness of disconnection of the affected hemisphere was evaluated in postoperative MRI. Disconnection lines were visually followed in each of three dimensional images. We checked particularly with care the complete sectioning of the genu and splenium of the corpus callosum, and the complete disconnection between the thalamus and surrounding cortices including the insula.

3. Results

Surgical procedure was completed without any intraoperative complication in all cases. Although we could obtain a good lateral view enough to vertically cut the lateral border of the thalamus in all patients, a small portion of the cingulate gyrus was excised in 2 infants with hemimegalencephaly to obtain a better view and a larger working space (Fig. 3). Postoperative course was uneventful in all patients. Blood loss during surgery was 50, 113, 136 and 150 mL in 4 infants and 160, 305 and 340 mL in 3 adults. No hypothalamic dysfunction including diabetes insipidus and poikilothermia was noted in any patients. There was no case that required transient CSF diversion or placement of CSF shunting. Seizure outcome was Engel's class I in 6 and class IV in 1. The patient whose outcome was class IV was hemimegalencephaly in whom postsurgical workup revealed residual epileptogenecity in the contralateral hemisphere.

Postoperative MRI revealed complete disconnection of affected hemisphere in all cases (Fig. 3).

4. Discussion

We reported our modification of Delalande's vertical hemispherotomy. While the original procedure devised by Delalande was an innovative procedure of hemispherotomy in minimizing brain resection [6], we thought that we could further improve it with minor modifications. One of the authors reviewed the hemispherotomy series at Tokyo Metropolitan Neurological Hospital for 37 children with malformation of cortical development [7]. In this study, the procedure was decomposed into a disconnection of the commissural fibers and a disconnection of the projection fibers, and elemental surgical procedures were compared in terms of the completeness of disconnection and the occurrence of complication (Fig. 4). For disconnection of the commissural fibers, we compared interhemispheric callosotomy used in two-stage hemispherotomy and transventricular callosotomy used in lateral hemispherotomy. Four of 19 cases of transventricular callosotomy were incomplete while none of 18 cases of interhemispheric callosotomy was incomplete. All of the four cases with incomplete transventricular callosotomy were hemimegalencephaly with the anomalous and asymmetric genu.

In Delalande's original method, callosotomy was performed in a parasagittal route that is similar to the interhemispheric route. Therefore, there may not be essential difference between our modification and Delalande's original, but we thought that staying in the midline decreased a risk of disorientation, particularly in anomalous midline structures often encountered in hemimegalencephaly, and particularly for surgeons who are used to interhemispheric callosotomy.

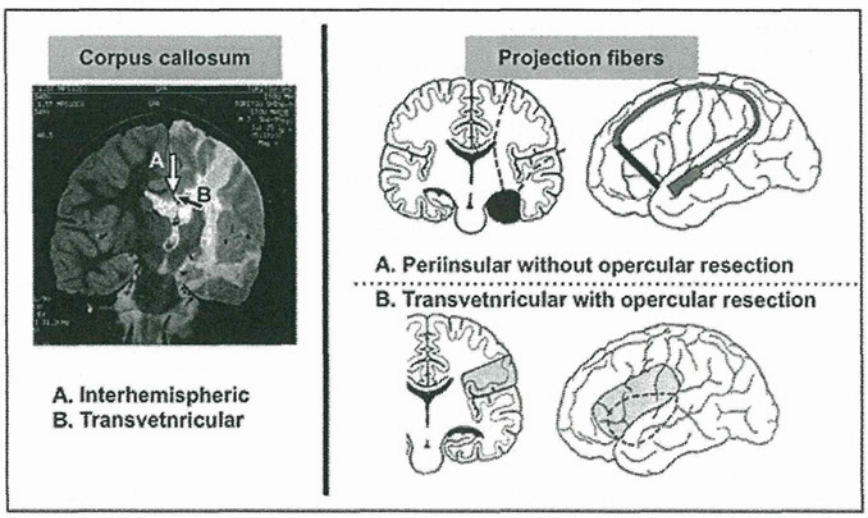

Fig. 4. The procedures of hemispherotomy are composed of disconnection of the corpus callosum and the projection fibers. For disconnection of the corpus callosum, interhemispheric callosotomy (left, A) and transventricular callosotomy (left, B) were compared. For disconnection of the projection fibers, periinsular hemispherotomy (right, A) and transopercular hemispherotomy (right, B) were compared.

Please cite this article in press as: Kawai K et al. Modification of vertical hemispherotomy for refractory epilepsy. Brain Dev (2013), http://dx.doi.org/10.1016/j.braindev.2012.12.013

The other major finding of the review was that the less brain resection results in the less complication associated with CSF circulation [7]. We compared the rate of postoperative CSF shunt or Ommaya reservoir among periinsular hemispherotomy and transopercular hemispherotomy [4]. The latter was devised by Shimizu and Maehara to obtain larger working space in hemimegalencephaly by resecting frontotemporoparietal operculums. 9% of 11 procedures without opercular resection required postoperative CSF diversion while 47% of 15 procedures with opercular resection required it, suggesting that less brain resection resulted in the smaller occurrence of postoperative CSF circulation complications.

Our modification changed the anterior disconnection plane more posteriorly than the Delalande's original by connecting the anterior end of the choroidal fissure to the anterior end of the foramen of Monro, instead of the former to the subcallosal area. It is unknown that the small difference of resection volume really contributed to the decreased occurrence of CSF complication, and this must be confirmed in further studies. However, this minor modification may have a merit in completely disconnecting the residual epileptic tissues in cases with dysplasia in posterior orbitofrontal regions [9], and in reducing blood loss from perforating arteries of the anterior and middle cerebral arteries by avoiding cutting into the caudate nucleus. Of course, these speculations must be confirmed by further experience.

In our modified procedure we cut into the hypothalamus. We first worried about the risk of hypothalamic dysfunction, but we did not observe any disturbance in fluid and ion balance, body temperature, and others. Conventional anatomical hemispherectomy resects the significant amount of the hypothalamus but no severe hypothalamic dysfunction was reported. Therefore, we may not need to worry about this complication.

In conclusion, though these were minor modifications, they further minimized brain resection and may serve for less invasiveness of procedure and improvement in completeness of disconnection and its confirmation during surgery.

References

[1] Rasmussen T. Hemispherectomy for seizures revisited. Can J Neurol Sci 1983;10:71–8.
[2] Villemure JG et al. Hemispherectomy. In: Engel JJ, editor. Surgical Treatment of the Epilepsies. New York: Raven Press Ltd.; 1993. p. 511–8.
[3] Villemure JG, Mascott CR. Peri-insular hemispherotomy: surgical principles and anatomy. Neurosurgery 1995;37:975–81.
[4] Shimizu H, Maehara T. Modification of peri-insular hemispherotomy and surgical results. Neurosurgery 2000;47:367–72 Discussion 372–3.
[5] Schramm J, Kral T, Clusmann H. Transsylvian keyhole functional hemispherectomy. Neurosurgery 2001;49:891–900 Discussion 900–1.
[6] Delalande O et al. From hemispherectomy to hemispherotomy. In: Lüders HO, Comair YG, editors. Epilepsy Surgery. Philadelphia: Lippincott Williams & Wilkins; 2001. p. 741–6.
[7] Kawai K, Shimizu H. Clinical outcome and comparison of surgical procedures in hemispherotomy for children with malformation of cortical development. Epilepsia 2004;45(Suppl. 7):168.
[8] Kawai K et al. Clinical outcomes after corpus callosotomy in patients with bihemispheric malformations of cortical development. J Neurosurg 2004;101:7–15.
[9] Mittal S et al. Intractable epilepsy after a functional hemispherectomy: important lessons from an unusual case. Case report. J Neurosurg 2001;94:510–4.

Please cite this article in press as: Kawai K et al. Modification of vertical hemispherotomy for refractory epilepsy. Brain Dev (2013), http://dx.doi.org/10.1016/j.braindev.2012.12.013

NeuroImage 65 (2013) 242–249

Contents lists available at SciVerse ScienceDirect

NeuroImage

journal homepage: www.elsevier.com/locate/ynimg

Characteristic profiles of high gamma activity and blood oxygenation level-dependent responses in various language areas

Naoto Kunii, Kyousuke Kamada *, Takahiro Ota [1], Kensuke Kawai, Nobuhito Saito

Department of Neurosurgery, The University of Tokyo, 7-3-1 Hongo, Bunkyo-ku, Tokyo 113-8655, Japan

ARTICLE INFO

Article history:
Accepted 24 September 2012
Available online 29 September 2012

Keywords:
Blood oxygenation level dependent
Electrocorticography
High gamma activity
Language
Oscillation

ABSTRACT

High gamma activity (HGA) has been shown to be positively correlated with blood oxygenation level-dependent (BOLD) responses in the primary cortices with simple tasks. It is, however, an open question whether the correlation is simply applied to the association areas related to higher cognitive functions. The aim of this study is to investigate quantitative correlation between HGA and BOLD and their spatial and temporal profiles during semantic processing. Thirteen patients with intractable epilepsy underwent fMRI and electrocorticography (ECoG) with a word interpretation task to evoke language-related responses. Percent signal change of BOLD was calculated at each site of ECoG electrode, which has power amplification of high gamma band (60–120 Hz) activity. We transformed locations of individual electrodes and brains to a universal coordination using SPM8 and made the quantitative comparisons on a template brain. HGAs were increased in several language-related areas such as the inferior frontal and middle temporal gyri and were positively correlated with BOLD responses. The most striking finding was different temporal dynamics of HGAs in the different brain regions. Whereas the frontal lobe showed longer-lasting HGA, the HGA-intensity on the temporal lobe quickly declined. The different temporal dynamics of HGA might explain why routine language-fMRI hardly detected BOLD in the temporal lobe. This study clarified different neural oscillation and BOLD response in various brain regions during semantic processing and will facilitate practical utilization of fMRI for evaluating higher-order cognitive functions not only in basic neuroscience, but also in clinical practice.

Introduction

A visualization technique of blood oxygenation level-dependent (BOLD) responses was developed as functional magnetic resonance imaging (fMRI) in the 1990s (Ogawa et al., 1990). Since then, fMRI has yielded a wealth of knowledge concerning various brain functions (Price, 2012). Meanwhile, it has been shown that fMRI activation includes a lot of subsidiary cortical areas unnecessary for actual implementation of a specific brain function. In particular, higher-order cognitive functions such as language seem to have wider supplementary areas, as several studies have shown that compared the fMRI results with electrocortical stimulation mapping (Bizzi et al., 2008; Kunii et al., 2011; Rutten et al., 2002). To utilize fMRI reliably in a clinical setting, we need to know in which situations the BOLD signal reflects the reality of neural activity. It is, therefore, of paramount importance to evaluate the concordance and dissociation between BOLD responses and underlying neuronal activity.

Power changes of oscillatory neuronal activities in various frequency ranges have recently received particular attention as physiological correlates of BOLD responses. Among them, the augmentation of high gamma activity (HGA) is assumed to reflect localized cortical processing and has been shown to be correlated with BOLD responses, mainly in the primary cortices such as the visual cortices of animals (Goense and Logothetis, 2008; Logothetis et al., 2001; Niessing et al., 2005) and the primary visual, auditory and motor cortices of humans (Hermes et al., 2011; Nir et al., 2007; Scheeringa et al., 2011). This assumption of HGA as a neural correlate of BOLD, that is, HGA–BOLD coupling, is supported by several basic studies as follows. Pharmacological (Hormuzdi et al., 2001; Traub et al., 2001), computer-simulation (Traub et al., 1997; Wang and Buzsaki, 1996) and electrophysiological studies (Cardin et al., 2009) suggested that HGA should be generated by synchronous post-synaptic potentials of fast-spiking GABAergic interneurons incorporated in a cortical assembly. On the other hand, approximately 74% of the energy budget of the brain was estimated to be devoted to post-synaptic potentials (Attwell and Iadecola, 2002). Taking these findings together, it is rational to assume that HGA could account for a large part of the blood oxygenation change.

* Corresponding author at: Department of Neurosurgery, Asahikawa Medical University, Asahikawa, Japan, 2-1, Midorigaoka-Higashi, Asahikawa, Hokkaido 078-8510, Japan. Fax: +81 166 68 2599.
E-mail address: kamady-k@umin.ac.jp (K. Kamada).
[1] Present address: Department of Neurosurgery, Tokyo Metropolitan Tama Medical Center, Tokyo, Japan, 2-8-29, Musashidai, Fuchu, Tokyo 183-8524, Japan.

1053-8119/$ – see front matter © 2012 Elsevier Inc. All rights reserved.
http://dx.doi.org/10.1016/j.neuroimage.2012.09.059

On the other hand, there are a limited number of studies that investigated HGA–BOLD coupling in the association cortex. Lachaux et al. (2007) showed a close spatial correspondence of the coupling using depth electrodes in frontotemporal regions under semantic paradigms. Ojemann et al. (2009) undertook a detailed estimation of HGA–BOLD coupling in the temporal association cortex and found that HGA is a significant regressor of BOLD. Conner et al. (2011) studied the correlation between various frequency bands and BOLD in various cortices using subdural grids and found positive and negative correlations of BOLD with HGA and beta band oscillation, respectively. Although recent studies have gradually elucidated the relationships between brain oscillations and BOLD, detailed analysis of HGA–BOLD coupling in the human association cortices is needed for further progress of neuroimaging and neuroscience fields.

From previous language-fMRI studies, it is known that the temporal language areas are less activated by the various semantic paradigms than the frontal language areas (Kamada et al., 2007; Kunii et al., 2011; Rutten et al., 2002; Veltman et al., 2000). Kamada et al. revealed that fMRI had a higher sensitivity to the frontal language activity while magnetoencephalography to the temporal language activity. Rutten et al. explained that complex tasks such as sentence reading might activate the receptive language functions in the temporal lobe. Despite practical importance of reproducibility in imaging studies, it remains almost unknown why different imaging modalities and language tasks induce spatially different responses. It is important to clarify the fundamental difference between frontal and temporal language dynamics by analysis of HGA–BOLD coupling.

In this study, we focused on spatial and quantitative relationships of HGA–BOLD coupling in language areas. The results should contribute to providing supportive evidence of the robustness of fMRI. In order to elucidate the fundamental neurophysiology of language networks, regional differences between HGA dynamics and fMRI activation were investigated.

Materials and methods

Subjects

This study included 23 patients with intractable epilepsy who had undergone implantation of subdural electrodes for diagnostic purposes at the University of Tokyo Hospital since December 2006. Nine patients were excluded because they had a low intelligence quotient (<70) or no chance of preoperative fMRI evaluation. All the patients underwent the Wada test to investigate language lateralization. One patient, who had bilateral language representation as determined by the Wada test, was excluded from further studies. As a result, we investigated 13 patients (5 men, 8 women) with left language dominance. Detailed demographic data are shown in Table 1.

Table 1
Patient demographic and clinical characteristics.

Patient no.	Age (years), sex	Etiology	VIQ	Epileptic focus
1	36, Male	Cortical dysplasia	82	Right frontal
2	50, Female	Cavernous malformation	91	Right temporal
3	40, Male	Unknown	85	Left temporal
4	33, Female	Cortical dysplasia	94	Left frontal
5	40, Male	Unknown	93	Right temporal
6	26, Female	Unknown	87	Right temporal
7	47, Female	Cortical dysplasia	88	Right temporal
8	24, Male	Cortical dysplasia	83	Left temporal
9	35, Female	Arachnoid cyst	107	Left temporal
10	21, Male	Middle fossa encephalocele	79	Left temporal
11	36, Female	Unknown	72	Left temporal
12	36, Female	Mesial temporal sclerosis	97	Left temporal
13	22, Female	Unknown	79	Right temporal

VIQ = verbal intelligence quotient.

This study was approved by the research ethics committee of the faculty of medicine, University of Tokyo (approval number 1797). Written informed consent was obtained from each patient or their family before they participated in the study.

Language-fMRI data acquisition

In all patients, fMRI was performed more than two months before electrode implantation. MR imaging was performed using a 3-tesla MR scanner with echo planar capabilities and a whole-head receive-only coil (Signa, General Electric, USA). During the experiments, foam cushions were used to immobilize the patient's head. Before the fMRI session, three-dimensional T1-weighted MR images (3D-MRI) of the subject's brain were obtained, which consisted of 136 sequential, 1.4-mm-thick axial slices with a resolution of 256×256 pixels in an FOV of 240 mm. fMRI was performed with a T2*-weighted echo planar imaging sequence (echo time: 35 ms, repetition time: 4000 ms, flip angle: 90 degrees, slice thickness: 4 mm, slice gap: 1 mm, field of view (FOV): 280 mm, matrix: 64×64, number of slices: 22). Owing to the different head sizes and positions of each patient, we selected a large FOV that could always contain the entire head, fixing the same center of the FOV on the x- and y-axes for all sessions. This enabled simple and exact co-registration of the different image sessions.

Each fMRI session consisted of three dummy scan volumes, three activation periods, and 4 baseline (rest) periods. During each period, 5 echo planar imaging volumes were collected, yielding a total of 38 imaging volumes. To obtain language-fMRI data, we used a kind of reading task called the word interpretation task as follows.

Word interpretation task

Visual stimuli were presented on a liquid crystal display monitor, with a mirror above the head coil allowing the patient to see the stimuli. In the reading periods, words consisting of three Japanese letters were presented in a 2000 ms exposure time with interstimulus intervals of 500 ms. All letter strings were white with a black background. The patients were instructed to read the presented word silently and categorize it into "abstract" or "concrete" based on the nature of the word. During the rest periods, the patients passively viewed random dots of destructured letters that had the same luminance as the stimuli so as to eliminate primary visual responses. All words for the semantic tasks were selected from common Japanese words listed in the electronic dictionary produced by the National Institute for Japanese Language.

Language-fMRI data analysis

The functional imaging data were preprocessed and analyzed with SPM8 (Wellcome Department of Imaging Neuroscience, London, UK), implemented in MATLAB (The Mathworks, Inc., Natick, MA). The functional scans were realigned, normalized onto a template brain and spatially smoothed using a Gaussian filter (8 mm kernel). Preprocessed data of each patient were analyzed with the standard general linear model (GLM) approach using boxcar predictors convolved with the canonical hemodynamic response function (Friston et al., 1995). Low-frequency noise was removed with a high-pass filter (128 Hz). A second-level random effects analysis was performed on the contrast images generated for each individual to identify brain regions showing reliable differences between reading and rest periods. A P value of 0.005 uncorrected threshold was used to estimate the t-map. The resulting t-map was superimposed over a three-dimensional template brain using MRIcroN software (second-level fMRI map) (http://www.sph.sc.edu/comd/rorden/mricron/).

We utilized percent signal change of BOLD (BOLD-SC) to quantify the BOLD responses for each individual. A BOLD-SC is defined as the maximum height of the time course estimated for a task condition,

divided by the average signal across the whole session within a region of interest (ROI), and multiplied by 100. We defined a sphere-type ROI with 10 mm radius at the center of each electrode. The ROI analysis was performed using the Mars-Bar region of interest toolbox for SPM available on the Web at http://marsbar.sourceforge.net (Brett et al., 2002).

ECoG data acquisition

Each patient underwent electrode implantation for 2 to 3 weeks before resection of epileptogenic foci. We used grid and strip-type subdural electrodes, which consisted of silastic sheets embedded with platinum electrodes (3 mm in diameter), and a 10 mm interelectrode interval (center to center) (Unique Medical, Tokyo, Japan). Electrode locations were determined from post-implantation CT and aligned to pre-implantation volumetric MRI using EMSE v5.3 software (Source Signal Imaging, San Diego, CA). The estimated registration accuracy is ±2.5 mm, without accounting for surgical or MR imaging geometrical distortion (Ossadtchi et al., 2010).

ECoG recordings for this study were performed at least 48 hours after the last epileptic seizures. We confirmed also that the patients were not in epileptic states during and immediately after the recordings. Each patient was seated on a bed with a reclining backrest in an electrically shielded room. A computer monitor was placed 100 cm from the patient. Visual stimuli were presented using a Stimuli Output Sequencer (NoruPro Light Systems Inc., Tokyo, Japan). The resulting ECoG were digitally recorded at a sampling rate of 400 Hz, using a 128-channel EEG system (BMSI 6000, Nicolet Biomedical Inc., Wisconsin). The band-pass filter for the data acquisition was set to 0.55–150 Hz. Electric triggers generated by the stimulus computer were simultaneously recorded with one of the EEG channels. A reference electrode was placed on the scalp at Cz (international 10–20 system). The stimuli for the language task consisted of the same words used in the word interpretation task of the fMRI session. All letter strings were presented for 350 ms with randomly variable interstimulus intervals, ranging between 2700 and 3300 ms. The words were displayed randomly, and each was presented once or twice, yielding 100 data epochs. The patients were instructed to read the words covertly and categorize them into "abstract" or "concrete."

ECoG data processing

All analyses of the ECoG data were performed using custom software written in Matlab R2008b. We focused on the electrodes on the lateral surface of the dominant hemisphere, which showed language-related activations on fMRI. The baseline and reading periods for all analyses were −600 to −100 ms pre-stimulus and 0 to 750 ms post-stimulus, respectively. On the basis of a visual inspection of the ECoG signals, epochs involving singular noises and epileptic spikes were excluded from further analysis. Fast Fourier transformation was performed every 1 Hz using 250 ms windows with 125 ms step sizes to obtain power spectral density estimates. A Hanning window was imposed on each data window to attenuate edge effects (Fig. 1A).

To obtain the power average across the high gamma range, we standardized the power spectral density estimates with respect to the 1500 ms data epochs consisting of pre- and post-stimulus 750 ms data epochs (Fig. 1B). This flattened out the spectral landscape, which allowed averaging across frequencies (Leuthardt et al., 2007). We defined a high gamma power change (HG-PC) as a standardized spectral power change from baseline to reading periods in a high-frequency band (60–120 Hz) (Fig. 1C). A *t*-test was performed to test whether the HG-PC was significantly larger than zero, and results were reported at $P<0.05$, Bonferroni-corrected for the number

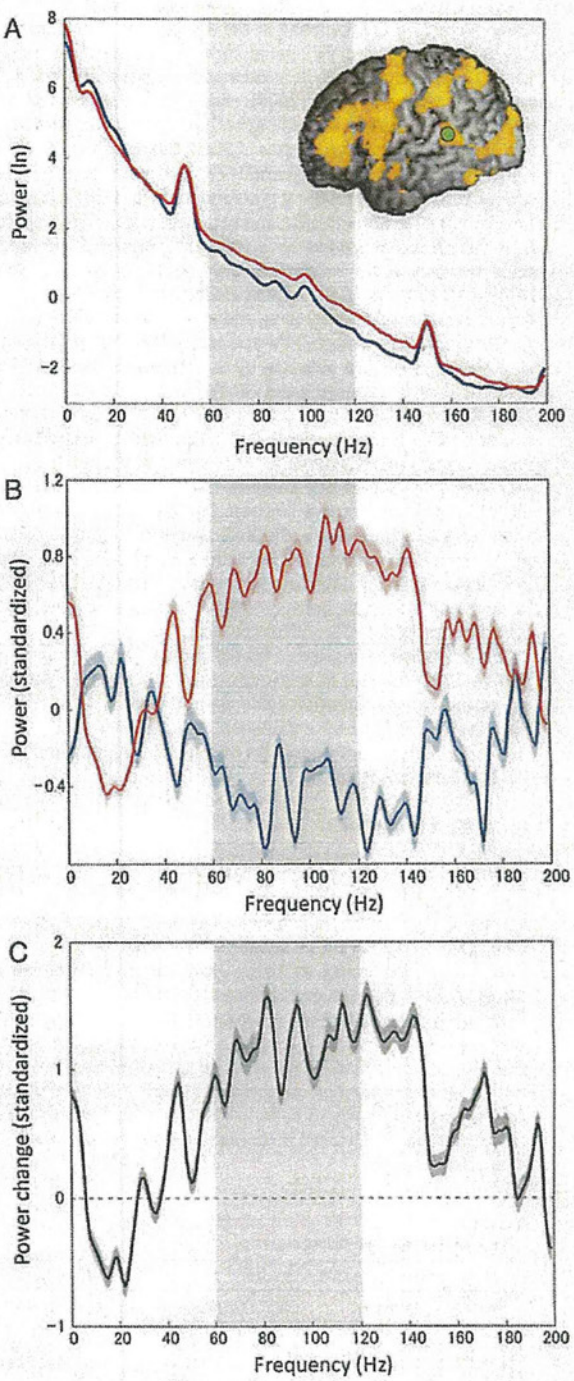

Fig. 1. Frequency profiles of an electrode (green dot on the left superior temporal gyrus). The light-gray zones indicate the high gamma frequency range (60–120 Hz). (A) Power spectral density functions in reading (red line) and rest (blue line) periods. The power was increased in the high gamma frequency range during the reading task. (B) Standardized power spectral density functions in reading and rest periods. Standardized power versus frequency was compared between the reading (red line) and rest periods (blue line). The shaded areas around the solid lines indicate standard errors of the mean values for each period. (C) Subtraction of the spectral density functions between reading and rest periods. The shaded area around the solid line indicates standard errors of the mean values.

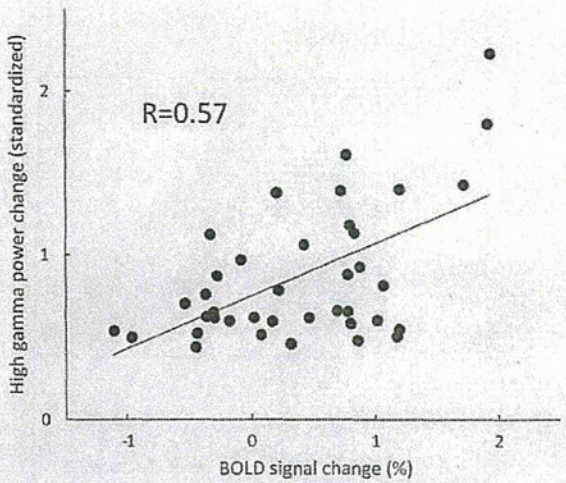

Fig. 2. Scatter plots of standardized high gamma power changes against BOLD signal changes. Regression analysis showed a positive correlation between them ($R=0.57$, $P=0.0002$).

of electrodes. The electrodes with significant or non-significant HG-PC are indicated as HGA(+) or HGA(−), respectively.

Statistical analysis

We tested whether BOLD responses correlated with HGAs. For each HGA(+) electrode, the BOLD-SC and HG-PC were calculated as described above. A linear regression model was fitted and tested for significance by an *F*-test.

For a better description of the relationship of HGA and BOLD in the frontal and temporal lobes, we made detailed comparisons across them: BOLD-SC responses between HGA(+) and HGA(−) sites, HG-PCs between the frontal and temporal lobes, and BOLD-SC between the frontal and temporal lobes, separately, according to the HGA profiles. To test the differences, we used Wilcoxon's rank sum test ($P<0.05$).

Electrode normalization and visualization on a template brain

To elucidate whether HGA(+) electrodes were located predominantly in the primary areas (e.g. sensori-motor cortex), we spatially normalized HGA(+) electrodes and displayed them on a template brain. A detailed procedure of electrode normalization is described elsewhere (Kunii et al., in press). This HGA distribution map was compared with the result of the second-level analysis of fMRI data.

Time-frequency analysis

To compare HGA dynamics in the frontal and temporal lobes, we further employed time-frequency analysis. The detailed procedure is described elsewhere (Kunii et al., in press). Briefly, we used spectrograms to estimate the energy density of the signals in the time-frequency plane. Short-time Fourier transformation was performed on the windowed epochs with 90% overlap. We performed a permutation test to determine *P* values for each time–frequency point of the spectrograms. The obtained *P*-value maps were corrected for multiple comparisons (false discovery rate correction, $P<0.05$).

To quantify the high gamma activity in the time course, we counted the number of frequency bins that displayed significant activity at each time point within the range of 60–120 Hz. We termed the resultant number the high gamma broadband index (HGBI).

Results

Finally, we investigated 478 electrodes, which covered the lateral surface of the dominant hemisphere on a template brain (Fig. 3A), and found 39 electrodes were HGA(+) (Fig. 3B). The mean values of BOLD-SC at HGA(+) and HGA(−) sites were 0.39 and 0.21, respectively, without a significant difference between them.

The regression analysis showed moderate correlation between HG-PC and BOLD-SC at HGA(+) sites ($R=0.57$, $P=0.0002$) (Fig. 2).

HGA(+) electrodes were localized in the inferior frontal, superior and middle temporal, and precentral gyri (premotor cortex and face-motor area) (Fig. 3B). A second-level fMRI map was displayed on the template brain (Fig. 3C). We compared distributions between BOLD activities and HGA(+) sites by visual inspection. In the frontal lobe, the distributions of the two activities generally matched. In the temporal lobe, however, considerable mismatch was observed, particularly in the superior temporal gyrus. HGAs were frequently localized in the superior temporal gyrus, whereas significant BOLD activities were not. Instead, wide BOLD activities appeared in the posterior inferior temporal gyrus, where ECoG electrodes were scarcely placed.

In order to explain the HGA–BOLD mismatch between the frontal and temporal lobes, we investigated the HGA profiles and found no significant difference of HG-PCs (Fig. 4B). In addition, there was no significant difference of frequency distribution in HGA on each lobe

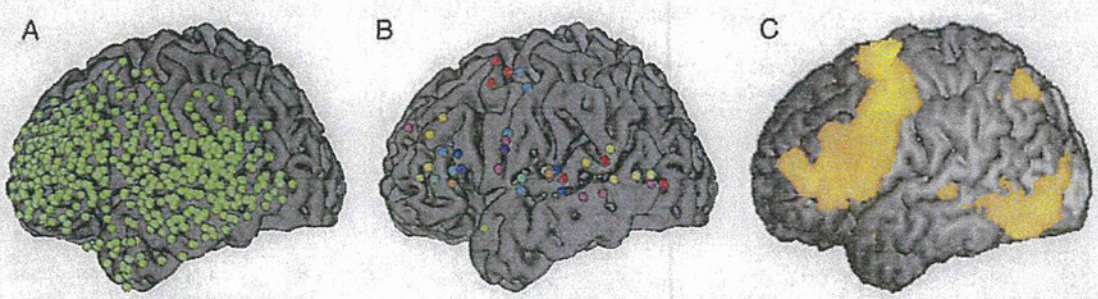

Fig. 3. Comparisons between distributions of high gamma activities (HGAs) and BOLD responses on a template brain. (A). All ECoG electrodes displayed on a template brain. The electrodes (green dots) on the template brain widely covered the lateral aspect of the left frontal and temporal lobes. (B) ECoG electrodes with significant HGA. Different colors of the electrodes indicate individual patients. The electrodes were mainly clustered on the inferior frontal, superior and middle temporal, and precentral gyri (premotor cortex and face-motor area). (C) A three-dimensional *t*-map of across-individual BOLD response displayed on a template brain. The BOLD responses were widely observed in the frontal lobe, which involves the inferior frontal and precentral gyri. There were additional activated areas in the inferior temporal gyrus, which were sparsely covered by ECoG electrodes.

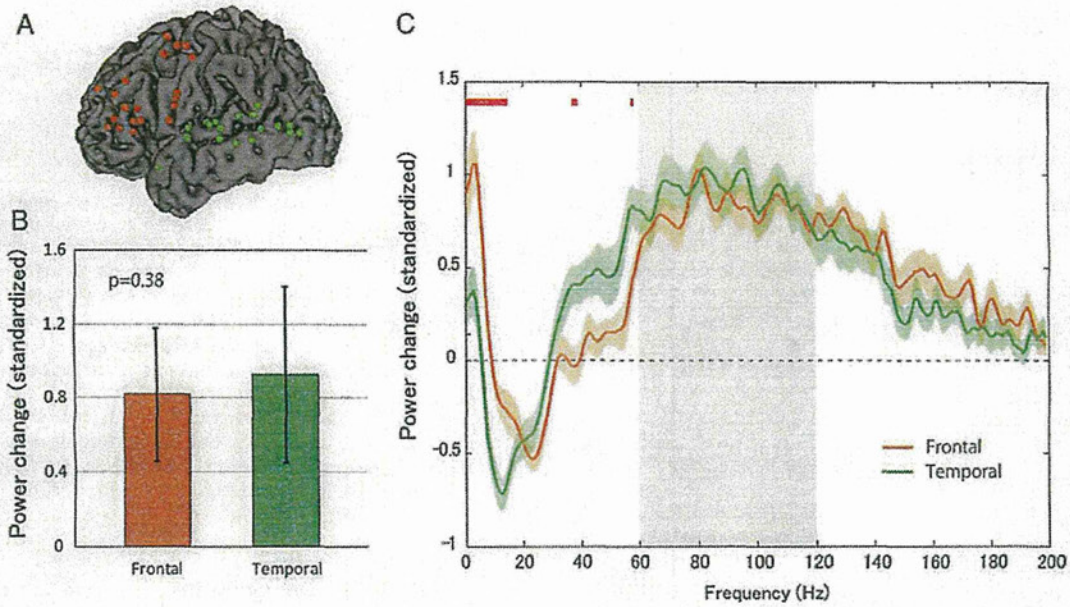

Fig. 4. Comparison of high gamma activity (HGA) between the frontal and temporal lobes. (A) Frontal (orange) and temporal (green) electrodes with significant HGAs. (B) Standardized power changes at the frontal (orange) and temporal (green) electrodes. There was no significant difference of high gamma activity between the frontal and temporal lobes. The error bars indicate the standard error of the mean and the *P*-value is based on Wilcoxon's rank sum test. (C) Spectral density functions of the standardized power changes in the frontal (orange) and temporal (green) lobes. Orange and green lines indicate the grand averages of spectral density functions in the frontal and temporal lobes, respectively. Red bars above the lines indicate significant differences of spectral density functions between frontal and temporal lobes ($P < 0.05$). Power increase in the theta range and decrease in the alpha range were stronger in the frontal and temporal lobes, respectively. There was no significant difference in the high gamma frequency range. The shaded area around the solid line indicates standard errors of the mean values. A light-gray zone indicates the high gamma frequency range (60–120 Hz).

(Fig. 4C). Note that we observed differences in other frequency ranges. Increased oscillatory activity in the theta range compared to the baseline (theta synchronization) was stronger in the frontal than the temporal lobe and decrease in the alpha range (alpha desynchronization) was dominantly observed in the temporal lobe.

We investigated whether the existence of HGA could affect the BOLD activities in the frontal and temporal lobes (Fig. 5). In HGA(+) sites, there was no significant difference between BOLD-SCs in the frontal and temporal lobes. In HGA(−) sites, on the other hand, BOLD-SCs were significantly higher in the frontal than in the temporal lobe ($P = 0.038$).

We then focused on temporal profiles of HGA in each lobe using time-frequency analyses. We investigated several brain regions such as the inferior frontal, precentral (premotor cortex and face motor area), middle and posterior superior temporal, and posterior middle temporal gyri, where the HGA(+) electrodes were clustered (Fig. 6). Each cluster showed characteristic temporal changes of HGA. In particular, the HGBI time courses of the temporal lobe had short latencies and declined rapidly at 500 ms with short duration. On the other hand, those of the frontal lobe had later onset with longer duration. Each lobe had independent and characteristic HGA dynamics.

Discussion

We observed language-related HGA and BOLD derived from 13 patients with intractable epilepsy and made detailed comparisons between them on a template brain. HGAs appeared not only in the primary motor area, but also in the language-related association cortices. Each region contained two or more HGA(+) electrodes, suggesting these areas showed the augmentation of HGAs consistently. In these HGA(+) regions, we demonstrated a positive correlation between HGAs and BOLD responses, and electrical oscillation could be a

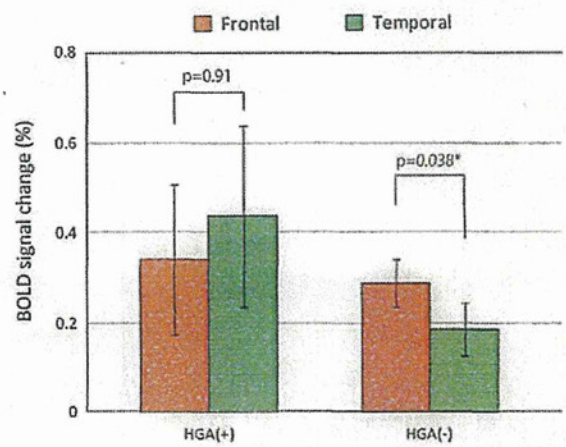

Fig. 5. Comparison of BOLD responses between the frontal (orange) and temporal (green) lobes. BOLD signal changes in each lobe were compared depending on high gamma activity (HGA) profiles (positive or negative). The BOLD responses with negative HGA were significantly higher in the frontal lobe than in the temporal lobe. There was no significant difference in the BOLD responses with positive HGA between the two lobes. The error bars indicate the standard error of the mean and the P-value is based on Wilcoxon's rank sum test.

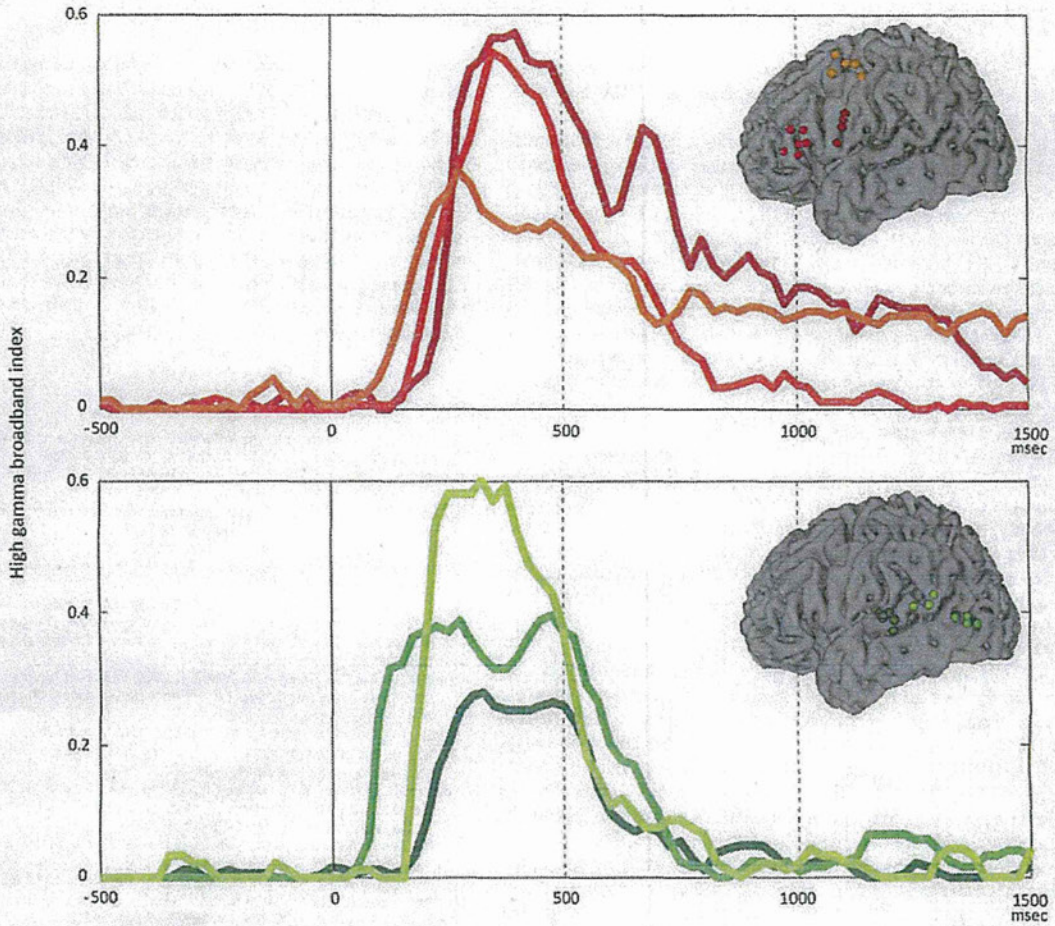

Fig. 6. Temporal dynamics of high gamma activity of noticeable electrode clusters in frontal and temporal lobes. Each line color corresponds to electrode color. *X* and *Y* axes indicate latency and high gamma broadband index (HGBI), respectively. HGBI in the frontal lobe lasted longer beyond 1000 ms. On the other hand, rapid decline of HGBI was observed after 500 ms in the temporal lobe.

physiological counterpart of BOLD signals. In addition, we found BOLD-HGA spatial mismatch and differences of HGA dynamics in the frontal and temporal lobes.

Previous studies have reported that the local field potentials (LFPs) positively correlated with BOLD responses in the primary cortices (e.g., visual, sensory, motor) of animals and humans (Goense and Logothetis, 2008; Hermes et al., 2011; Logothetis et al., 2001; Niessing et al., 2005; Nir et al., 2007; Scheeringa et al., 2011). Such LFP–BOLD coupling is assumed to be a measurable counterpart of neurovascular coupling, which is of paramount importance in interpreting the results of fMRI in neuroimaging research and clinical situations. The aim of this study is to clarify the neurovascular coupling in the human association cortex (language-related) by analyzing neuronal oscillations represented by HGA. Although LFP–BOLD coupling in the primary cortical areas was robust, some researchers have raised concerns over dissociation between LFPs and BOLD signals in other cortical areas (Arne, 2010). In fact, we observed no significant difference of BOLD responses between HGA(+) and HGA(−) sites, meaning that there were considerable BOLD responses without HGAs in association cortices. This finding seemed to reflect a wider distribution of hemodynamic BOLD responses around the corresponding electrical activities, which might have caused difficulties in demonstrating HGA–BOLD coupling in association cortices. In this study, we showed that HGAs were positively correlated with BOLD responses by including only BOLD responses at HGA(+) sites. We believe that our findings provide supportive evidence to elucidate HGA–BOLD coupling in association cortices.

The fMRI group analysis showed a spatial dissociation between BOLD responses and HGAs in the temporal lobe. Our study showed the reading task induced less BOLD responses in the temporal lobe, which was in line with the findings of previous studies (Kamada et al., 2007; Kunii et al., 2011; Rutten et al., 2002; Veltman et al., 2000). In order to determine the reasons for the spatial dissociation of HGA–BOLD coupling in the temporal lobe, we made detailed comparisons of HGA between the frontal and temporal lobes. The two lobes showed no significant difference of power spectral density in the high gamma band. Therefore, it might be hard to fully explain the dissociation of HGA and BOLD distribution between frontal and temporal lobes only by spectral characteristics of HGA. Interestingly, the BOLD responses in HGA(−) sites were significantly weaker in the temporal than in the frontal lobe. We speculated that BOLD responses in HGA(−) sites were more widely distributed around HGA(+) sites in the frontal than in the temporal lobe. In order to explain our hypothesis, we considered that the most important facts were HGA temporal profiles, assuming that prolonged electrical activation could evoke wider hemodynamic responses. According to the time-frequency analysis, the HGAs in the frontal lobe tended to be

longer-lasting than those in the temporal lobe. Such different temporal patterns of HGAs in each lobe might have generated the different BOLD responses around the functional epicenters, which could have led to the dissociation of the spatial distributions of HGAs and BOLD responses.

In this study, we used the word interpretation task, in which semantic decisions were needed after covert word reading. The inferior frontal lobe is strongly related with executive roles in semantic decisions (Badre and Wagner, 2007; Binder et al., 2009; Fiez, 1997; Martin et al., 1995, 1996; Noppeney et al., 2004; Thompson-Schill et al., 1997; Wagner et al., 2001). It seems that our task effectively induced HGA in the frontal association cortices, which might be the key for the excellent overall HGA–BOLD coupling. Wu et al., reported picture naming task elicited wider gamma oscillations in temporo-parietal regions than simple word reading (Wu et al., 2011). In this sense, picture naming task might provide additional information on the relationship between HGA and BOLD responses.

HGAs, which seem to reflect the excitement of local neural assemblies, are only a part of various electrical activities generated in a human brain. Although we mainly investigated the HGA as a plausible candidate of electrophysiological correlates for BOLD responses, some parts of the BOLD responses could be attributable to the power changes in other frequency ranges. Scheeringa et al. (2011) performed simultaneous recording of EEG and fMRI and found that gamma power increase and alpha-beta power decrease in EEG were positively and negatively correlated with BOLD responses in the primary visual area, respectively (Scheeringa et al., 2011). Hermes et al. (2011), in their study on LFP–BOLD coupling in motor function, suggested that BOLD signal change was largely induced by high gamma power increase and alpha-beta power decrease in the primary motor area. Furthermore, Khursheed et al. (2011) stressed that theta power decrease had the most negative correlation with BOLD responses in working memory on the frontal lobe. On the basis of previous studies and our own, HGA–BOLD coupling is a promising key to identify complex human brain functions. Despite the strong correlation of HGA and BOLD signal in our study, it would be necessary to analyze other frequency ranges of electrical activities for further understanding.

Brain regions might have different hemodynamic responsive function (HRF) according to different tasks (Kruggel and von Cramon, 1999). BOLD responses obtained by block-design fMRI paradigms, however, do not reflect such regional differences of HRF. Most of the previous studies including ours on LFP–BOLD coupling have used block-design paradigms (Hermes et al., 2011; Logothetis et al., 2001; Ojemann et al., 2009) because of the high signal-to-noise ratio. Event-related fMRI paradigms, which can detect transient variations in hemodynamic responses, might allow the temporal characterization of BOLD signal changes. This technique, however, has lower signal-to-noise ratio than the block-design fMRI paradigm in the present system setting. It would be possible to make detailed analysis of the coupling if we were to use novel fMRI techniques with higher signal-to-noise ratio and temporal resolution.

Conclusion

This study provided an important bridge between the functional brain networks revealed by BOLD responses and the underlying neurophysiology. We found that there were different temporal profiles of HGA in the frontal and temporal language areas. The longer-lasting HGA contributed to dominant fMRI activation in the frontal lobe, whereas the short-duration HGA reflected poor BOLD signals in the temporal lobe. Such different temporal patterns of HGAs in each lobe might have generated the different BOLD responses around the functional epicenters, which could have led to the dissociation of the spatial distributions of HGAs and BOLD responses.

We believe this work will facilitate practical utilization of fMRI for evaluating higher-order cognitive functions not only in neuroscience research but also in a clinical context.

Acknowledgments

This work was supported in part by the Japan Epilepsy Research Foundation, a grant from the Suhara Memorial Foundation, Grant-in-Aid No. 21390405 and 24390337 for Scientific Research (B) from the Japan Society for the Promotion of Science, Grant-in-Aid No. 23659679 for Challenging Exploratory Research from Ministry of Education, Culture, Sports, Science and Technology of Japan (MEXT), Grant-in-Aid No. 23119701 for Scientific Research on Innovative Areas, "Face perception and recognition" from MEXT, a Research Grant for "Decoding and controlling brain information" from the Japan Science and Technology Agency, and a Grant H23—Nervous and Muscular-General-003 for Comprehensive Research on Disability, Health and Welfare from the Ministry of Health, Labour and Welfare of Japan.

References

Arne, E., 2010. How and when the fMRI BOLD signal relates to underlying neural activity: the danger in dissociation. Brain Res. Rev. 62, 233–244.
Attwell, D., Iadecola, C., 2002. The neural basis of functional brain imaging signals. Trends Neurosci. 25, 621–625.
Badre, D., Wagner, A.D., 2007. Left ventrolateral prefrontal cortex and the cognitive control of memory. Neuropsychologia 45, 2883–2901.
Binder, J.R., Desai, R.H., Graves, W.W., Conant, L.L., 2009. Where is the semantic system? A critical review and meta-analysis of 120 functional neuroimaging studies. Cereb. Cortex 19, 2767–2796.
Bizzi, A., Blasi, V., Falini, A., Ferroli, P., Cadioli, M., Danesi, U., Aquino, D., Marras, C., Caldiroli, D., Broggi, G., 2008. Presurgical functional MR imaging of language and motor functions: validation with intraoperative electrocortical mapping. Radiology 248, 579–589.
Brett, M., Anton, J., Valbregue, R., Poline, J., 2002. Region of interest analysis using an SPM toolbox. 8th International Conference on Functional Mapping of the Human Brain, Sendai, Japan.
Cardin, J.A., Carlen, M., Meletis, K., Knoblich, U., Zhang, F., Deisseroth, K., Tsai, L.H., Moore, C.I., 2009. Driving fast-spiking cells induces gamma rhythm and controls sensory responses. Nature 459, 663–667.
Conner, C.R., Ellmore, T.M., Pieters, T.A., DiSano, M.A., Tandon, N., 2011. Variability of the relationship between electrophysiology and BOLD-fMRI across cortical regions in humans. J. Neurosci. 31, 12855–12865.
Fiez, J.A., 1997. Phonology, semantics, and the role of the left inferior prefrontal cortex. Hum. Brain Mapp. 5, 79–83.
Friston, K.J., Holmes, A.P., Poline, J.B., Grasby, P.J., Williams, S.C., Frackowiak, R.S., Turner, R., 1995. Analysis of fMRI time-series revisited. Neuroimage 2, 45–53.
Goense, J.B., Logothetis, N.K., 2008. Neurophysiology of the BOLD fMRI signal in awake monkeys. Curr. Biol. 18, 631–640.
Hermes, D., Miller, K.J., Vansteensel, M.J., Aarnoutse, E.J., Leijten, F.S., Ramsey, N.F., 2011. Neurophysiologic correlates of fMRI in human motor cortex. Hum. Brain Mapp. 33, 1689–1699.
Hormuzdi, S.G., Pais, I., LeBeau, F.E., Towers, S.K., Rozov, A., Buhl, E.H., Whittington, M.A., Monyer, H., 2001. Impaired electrical signaling disrupts gamma frequency oscillations in connexin 36-deficient mice. Neuron 31, 487–495.
Kamada, K., Sawamura, Y., Takeuchi, F., Kuriki, S., Kawai, K., Morita, A., Todo, T., 2007. Expressive and receptive language areas determined by a non-invasive reliable method using functional magnetic resonance imaging and magnetoencephalography. Neurosurgery 60, 296–305 (discussion 305–296).
Khursheed, F., Tandon, N., Tertel, K., Pieters, T.A., Disano, M.A., Ellmore, T.M., 2011. Frequency-specific electrocorticographic correlates of working memory delay period fMRI activity. Neuroimage 56, 1773–1782.
Kruggel, F., von Cramon, D.Y., 1999. Temporal properties of the hemodynamic response in functional MRI. Hum. Brain Mapp. 8, 259–271.
Kunii, N., Kamada, K., Ota, T., Greenblatt, R.E., Kawai, K., Saito, N., in press. The dynamics of language-related high-gamma activity assessed on a spatially-normalized brain. Clin. Neurophysiol. http://dx.doi.org/10.1016/j.clinph.2012.06.006.
Kunii, N., Kamada, K., Ota, T., Kawai, K., Saito, N., 2011. A detailed analysis of functional magnetic resonance imaging in the frontal language area—a comparative study with extraoperative electrocortical stimulation. Neurosurgery 69, 590–596 (discussion 596–597).
Lachaux, J.P., Fonlupt, P., Kahane, P., Minotti, L., Hoffmann, D., Bertrand, O., Baciu, M., 2007. Relationship between task-related gamma oscillations and BOLD signal: new insights from combined fMRI and intracranial EEG. Hum. Brain Mapp. 28, 1368–1375.
Leuthardt, E.C., Miller, K., Anderson, N.R., Schalk, G., Dowling, J., Miller, J., Moran, D.W., Ojemann, J.G., 2007. Electrocorticographic frequency alteration mapping: a clinical technique for mapping the motor cortex. Neurosurgery 60, 260–270 (discussion 270–261).
Logothetis, N.K., Pauls, J., Augath, M., Trinath, T., Oeltermann, A., 2001. Neurophysiological investigation of the basis of the fMRI signal. Nature 412, 150–157.
Martin, A., Haxby, J.V., Lalonde, F.M., Wiggs, C.L., Ungerleider, L.G., 1995. Discrete cortical regions associated with knowledge of color and knowledge of action. Science 270, 102–105.

Martin, A., Wiggs, C.L., Ungerleider, L.G., Haxby, J.V., 1996. Neural correlates of category-specific knowledge. Nature 379, 649–652.
Niessing, J., Ebisch, B., Schmidt, K.E., Niessing, M., Singer, W., Galuske, R.A., 2005. Hemodynamic signals correlate tightly with synchronized gamma oscillations. Science 309, 948–951.
Nir, Y., Fisch, L., Mukamel, R., Gelbard-Sagiv, H., Arieli, A., Fried, I., Malach, R., 2007. Coupling between neuronal firing rate, gamma LFP, and BOLD fMRI is related to interneuronal correlations. Curr. Biol. 17, 1275–1285.
Noppeney, U., Phillips, J., Price, C., 2004. The neural areas that control the retrieval and selection of semantics. Neuropsychologia 42, 1269–1280.
Ogawa, S., Lee, T.M., Kay, A.R., Tank, D.W., 1990. Brain magnetic resonance imaging with contrast dependent on blood oxygenation. Proc. Natl. Acad. Sci. U. S. A. 87, 9868–9872.
Ojemann, G.A., Corina, D.P., Corrigan, N., Schoenfield-McNeill, J., Poliakov, A., Zamora, L., Zanos, S., 2009. Neuronal correlates of functional magnetic resonance imaging in human temporal cortex. Brain 133, 46–59.
Ossadtchi, A., Greenblatt, R.E., Towle, V.L., Kohrman, M.H., Kamada, K., 2010. Inferring spatiotemporal network patterns from intracranial EEG data. Clin. Neurophysiol. 121, 823–835.
Price, C.J., 2012. A review and synthesis of the first 20years of PET and fMRI studies of heard speech, spoken language and reading. Neuroimage 62, 816–847.
Rutten, G.J., Ramsey, N.F., van Rijen, P.C., Noordmans, H.J., van Veelen, C.W., 2002. Development of a functional magnetic resonance imaging protocol for intraoperative localization of critical temporoparietal language areas. Ann. Neurol. 51, 350–360.
Scheeringa, R., Fries, P., Petersson, K.M., Oostenveld, R., Grothe, I., Norris, D.G., Hagoort, P., Bastiaansen, M.C., 2011. Neuronal dynamics underlying high- and low-frequency EEG oscillations contribute independently to the human BOLD signal. Neuron 69, 572–583.
Thompson-Schill, S.L., D'Esposito, M., Aguirre, G.K., Farah, M.J., 1997. Role of left inferior prefrontal cortex in retrieval of semantic knowledge: a reevaluation. Proc. Natl. Acad. Sci. U. S. A. 94, 14792–14797.
Traub, R.D., Jefferys, J.G., Whittington, M.A., 1997. Simulation of gamma rhythms in networks of interneurons and pyramidal cells. J. Comput. Neurosci. 4, 141–150.
Traub, R.D., Kopell, N., Bibbig, A., Buhl, E.H., LeBeau, F.E., Whittington, M.A., 2001. Gap junctions between interneuron dendrites can enhance synchrony of gamma oscillations in distributed networks. J. Neurosci. 21, 9478–9486.
Veltman, D.J., Friston, K.J., Sanders, G., Price, C.J., 2000. Regionally specific sensitivity differences in fMRI and PET: where do they come from? Neuroimage 11, 575–588.
Wagner, A.D., Pare-Blagoev, E.J., Clark, J., Poldrack, R.A., 2001. Recovering meaning: left prefrontal cortex guides controlled semantic retrieval. Neuron 31, 329–338.
Wang, X.J., Buzsaki, G., 1996. Gamma oscillation by synaptic inhibition in a hippocampal interneuronal network model. J. Neurosci. 16, 6402–6413.
Wu, H.C., Nagasawa, T., Brown, E.C., Juhasz, C., Rothermel, R., Hoechstetter, K., Shah, A., Mittal, S., Fuerst, D., Sood, S., Asano, E., 2011. Gamma-oscillations modulated by picture naming and word reading: intracranial recording in epileptic patients. Clin. Neurophysiol. 122, 1929–1942.

Clinical Neurophysiology 124 (2013) 91–100

Contents lists available at SciVerse ScienceDirect

Clinical Neurophysiology

journal homepage: www.elsevier.com/locate/clinph

The dynamics of language-related high-gamma activity assessed on a spatially-normalized brain

Naoto Kunii [a], Kyousuke Kamada [b,*], Takahiro Ota [a], Richard E. Greenblatt [c], Kensuke Kawai [a], Nobuhito Saito [a]

[a] Department of Neurosurgery, The University of Tokyo, Tokyo, Japan
[b] Department of Neurosurgery, Asahikawa Medical University, Asahikawa, Japan
[c] Source Signal Imaging Inc., San Diego, CA, USA

ARTICLE INFO

Article history:
Accepted 8 June 2012
Available online 12 July 2012

Keywords:
Electrocorticography (ECoG)
Event-related synchronization
High gamma activity
Language processing
Spatial normalization

HIGHLIGHTS

- We made spatial normalization of 1512 intracranial electrodes in 21 patients with intractable epilepsy to identify typical dynamics of semantic processing.
- Word interpretation task evoked high gamma activity (HGA) at 200 ms after stimulus onset on the posterior temporal language area and alternatively at 400 ms on the frontal language area, following the initial HGA of bilateral fusiform gyri.
- The novel ECoG-normalization technique evolved visualization of electrophysiological dynamics related to semantic processing among individual subjects.

ABSTRACT

Objective: We developed a novel technique of spatial normalization of subdural electrode positions across subjects and assessed the spatial–temporal dynamics of high-gamma activity (HGA) in the dominant hemisphere elicited by three distinct language tasks.
Methods: The normalization process was applied to 1512 subdural electrodes implanted in 21 patients with intractable epilepsy. We projected each task-related HGA profile onto a normalized brain.
Results: The word interpretation task initially elicited HGA augmentation in the bilateral fusiform gyri at 100 ms after stimulus onsets, subsequently in the left posterior middle temporal gyrus, in the left ventral premotor cortex at 200 ms and in the left middle and left inferior frontal gyri at 300 ms and after. The picture naming task elicited HGA augmentation in few sites in the left frontal lobe. The verb generation task elicited HGA in the left superior temporal gyrus at 100–600 ms. Common HGA augmentation elicited by all three tasks was noted in the left posterior-middle temporal and left ventral premotor cortices.
Conclusions: The spatial–temporal dynamics of language-related HGA were demonstrated on a spatially-normalized brain template.
Significance: This study externally validated the spatial and temporal dynamics of language processing suggested by previous neuroimaging and electrophysiological studies.

1. Introduction

Language functions are generated by complex neural networks. To obtain better understanding of language mechanisms, it is necessary to make detailed maps using functional imaging and electrophysiological techniques. In particular, fine-scale time series analysis of the whole brain has great potential for the elucidation of neural networks.

Numerous lesional and hemodynamic studies have provided information about language networks (Binder et al., 2009; Dronkers et al., 2004; Price, 2010; Vigneau et al., 2006). In addition to the classical Wernicke's and Broca's areas, recent studies have found several language-related epicenters throughout the whole brain. The regions that are activated depend on the cognitive function being performed, for example, various areas of the brain have been found to be associated with orthography (Binder et al., 2006; Cohen et al., 2002; Tsapkini and Rapp, 2010), phonology (Binder et al., 2000; Buchsbaum et al., 2001; Rauschecker, 1998),

* Corresponding author. Address: Department of Neurosurgery, Asahikawa Medical University, 2-1, Midorigaoka-Higashi, Asahikawa, Hokkaido 078-8510, Japan. Tel.: +81 166 68 2594; fax: +81 166 68 2599.
E-mail address: kamady-k@umin.ac.jp (K. Kamada).

1388-2457/$36.00
http://dx.doi.org/10.1016/j.clinph.2012.06.006

lexico-semantic memory (Martin et al., 1995, 1996; Moore and Price, 1999; Noppeney et al., 2005), semantic selection/decisions (Badre and Wagner, 2007; Noppeney et al., 2004; Thompson-Schill et al., 1999; Wagner et al., 2001), speech production/perception (D'Ausilio et al., 2009; Hickok, 2001; Hickok et al., 2003; Pulvermuller et al., 2006; Wilson et al., 2004), syntax and sentence level comprehension (Friederici et al., 2003; Hashimoto and Sakai, 2002; Homae et al., 2002, 2003; Humphries et al., 2001; Ni et al., 2000), and verbal working memory (Champod and Petrides, 2007, 2010; Hickok et al., 2003; Jonides et al., 1998; Ravizza et al., 2004; Tsukiura et al., 2001). Although multiple epicenters have been found, it is difficult to elucidate the time course of the brain activity of distributed language areas and the dynamics of the language network. This is due to the technical limitations of hemodynamic studies such as positron emission computed tomography (PET) and functional MRI (fMRI), which have insufficient temporal resolution to describe the dynamics of neural activity.

On the other hand, electroencephalography (EEG) and magnetoencephalography (MEG) have been used to record event-related responses at high time resolution; i.e., event-related potentials (ERP) and event-related fields (ERF), respectively. Using these techniques, previous groups have demonstrated semantic responses within 200 ms of letter presentation for primary perception and within about 400 ms for letter cognition (Dhond et al., 2007; Salmelin et al., 1994; Vartiainen et al., 2009). However, questions remain about how to solve inverse problems, which interfere with source localization. In fact, there have been considerable disagreements about the origins of certain components (e.g., N400) (Curran et al., 1993; Halgren et al., 2002; Helenius et al., 1998; Johnson and Hamm, 2000; Maess et al., 2006; Pylkkanen and McElree, 2007; Tse et al., 2007; Uusvuori et al., 2008).

In the last few years, increasing effort has been made to assess brain oscillatory activity such as event-related synchro/desynchronization (ERS/ERD) using intracranial electrodes. Event-related augmentation of the ongoing EEG has been referred to as ERS, and augmentation of high gamma activity (HGA) at >50 Hz is generally considered to reflect cortical activation (Crone et al., 1998; Pfurtscheller and Lopes da Silva 1999).

Distributions of HGA augmentation display strong correlations with various functions, including motor (Crone et al., 1998; Leuthardt et al., 2007; Miller et al., 2007), auditory (Crone et al., 2001a; Edwards et al., 2005; Sinai et al., 2009; Trautner et al., 2006), visual (Lachaux et al., 2005; Tanji et al., 2005), language (Brown et al., 2008; Crone et al., 2001b; Sinai et al., 2005; Wu et al., 2011, 2010), episodic memory (Sederberg et al., 2007), working memory (Axmacher et al., 2007; Howard et al., 2003; Meltzer et al., 2008; van Vugt et al., 2010), and attention functions (Jung et al., 2008; Ray et al., 2008; Tallon-Baudry et al., 2005). Furthermore, studies of HGA can achieve both high spatial and temporal resolution. Therefore, analyzing HGA dynamics is one of the most powerful approaches for studying complex neural networks (Canolty et al., 2007; Edwards et al., 2010; Mainy et al., 2008).

One practical issue with this technique is the positioning of intracranial electrodes. Since it is impossible to control the electrode positions for research purposes from an ethical point of view, each patient is monitored with a different number of electrodes, and there are also inter-individual differences in their locations. As a result, consistent HGA dynamics are rarely obtained because of inter-individual variations in electrode positioning.

In order to overcome these limitations, we spatially normalized individual brains and the subdural electrodes of patients with intractable epilepsy and superimposed 1512 electrodes of the dominant hemisphere onto a normalized brain. We hypothesized that this novel method could allow us to demonstrate representative HGA patterns for various semantic tasks such as word interpretation, picture naming, and verb generation.

2. Subjects and methods

2.1. Subjects

We recorded ECoG in 34 patients with intractable epilepsy, who underwent subdural electrode implantation for diagnostic purposes at the University of Tokyo Hospital between May 2005 and November 2010. During the recording, we instructed the patients to perform 3 language tasks, word interpretation, picture naming, and verb generation. Thirteen patients were excluded because of a low intelligence quotient (<70) ($n = 9$), young age (<15) ($n = 1$), a lack of electrodes in the left hemisphere ($n = 1$), low signal quality ($n = 1$), or continuous epileptic activity ($n = 1$). As a result, we restricted this analysis to 21 patients (8 men, 13 women). Before the epilepsy surgery, we confirmed which hemisphere was dominant for language processes in each individual using the Wada test or a combination of fMRI and MEG, as described elsewhere (Kamada et al., 2007). There was no case in which the right hemisphere was dominant for language processes.

We used grid and strip type subdural electrodes, which consisted of silastic sheets embedded with platinum electrodes (3 mm in diameter), and a 10 mm inter-electrode interval (center to center) (Unique Medical, Tokyo, Japan). Since the purpose of this study was to elucidate the language dynamics in the dominant hemisphere, we excluded ECoG electrodes on the lateral surface of the right hemisphere.

This study was approved by the institutional review board of our institute. Written informed consent was obtained from each patient or their family after a detailed explanation of the ECoG and language evaluation procedures.

2.2. ECoG recording

2.2.1. Data acquisition

Each patient was seated on a bed with a reclining backrest in a quiet, electrically shielded room. A computer monitor was placed 100 cm from the patient. Stimuli were then presented using a Stimuli Output Sequencer (NoruPro Light Systems Inc., Tokyo, Japan).

The resultant ECoG were digitally recorded at a sampling rate of 400 Hz, using a 128 channel EEG system (BMSI 6000, Nicolet Biomedical Inc., Wisconsin). The band-pass filter for the data acquisition was set to 0.55–150 Hz. Electric triggers generated by the stimulus computer were simultaneously recorded by one of the channels.

A reference electrode was placed on the scalp at Cz (international 10–20 system).

2.2.2. Language tasks

Word interpretation (WI) task: The stimuli for the word interpretation task consisted of three-letter words. All letter strings were white with a black background and presented for 350 ms with a randomly variable inter-stimulus intervals, ranging between 2700 and 3300 ms. The words were displayed randomly, and each was presented once or twice, yielding 100 data epochs. The patients were instructed to covertly categorize the presented words into "abstract" or "concrete".

Picture naming (PN) task: The 100 stimuli used for the picture naming task consisted of 42 color illustrations of familiar objects. They were presented for 1000 ms with an inter-stimulus interval ranging between 2700 and 3300 ms. The patient was requested to silently name each presented object.

Verb generation (VG) task: Common concrete nouns spoken by a native Japanese speaker were presented by the computer. The twenty stimuli were presented in random order to generate 100

data epochs. The duration range of the auditory stimuli was <500 ms, and the inter-stimulus intervals varied randomly from 2700 to 3300 ms. The patient was instructed to silently generate a verb related to each presented noun.

2.3. Data analysis

2.3.1. ECoG data processing

All analyses of the ECoG data were performed using custom software written in Matlab R2008b (The Mathworks, Inc., Natick, MA). We divided the continuous ECoG into 2 s epochs (0.5 s before and 1.5 s after stimulus onset) with an additional 0.125 s on both sides of each epoch to prevent 'edge effect' artifacts from clouding the results. Based on a visual inspection of the ECoG signals, trials involving excessive epileptic activity were excluded from further analysis.

2.3.2. Time–frequency analysis

We used spectrograms to estimate the energy density of the signals in the time–frequency plane (Makeig, 1993; Zygierewicz et al., 2005), as described below: We divided the signal, $s(t)$, into overlapping epochs, each of which was multiplied by the window-function $w(t)$. Then, the Fourier transformation was performed on the windowed epochs, providing a frequency resolution dependent on the epoch length. The short-time Fourier transform (STFT) of signal $s(t)$ was given by:

$$F_s(u,f)\int_{-\infty}^{\infty} s(t)\omega^*(t-u)e^{-2\pi ift}dt \quad (1)$$

We used the following Hamming window:

$$w(t) = 0.54 - 0.46\cos\left(2\pi\frac{t}{T}\right) \quad (2)$$

where T was the window length. We then obtained a spectrogram by squaring the modulus of the STFT.

Each epoch of 800 time points was comprised of 80 Hamming-windowed, 100-point data windows with 90% overlap. For spectral interpolation, we applied zero-padding to the windowed time series, thus the output consisted of 100 frequency bins with width of 2 Hz. As a result, we obtained N time–frequency power distribution maps composed of 100 frequency bins, each of which was derived from 20 pre-stimulus and 60 post-stimulus time-series data points, where N represented the number of trials for each task.

2.3.3. Permutation test

We performed a permutation test to determine P values for each time–frequency point under the null hypothesis that there is no difference between the power value at a post-stimulus time–frequency point and the mean power value of the same frequency bin at the pre-stimulus baseline. The P value for each time–frequency point was obtained as follows (see Appendix A for more detail).

N mean power values at the pre-stimulus baseline and N time–frequency power values at a post-stimulus time–frequency point were pooled together and then 999 iterations were randomly shuffled and partitioned into two series of the same size as the original series. Averaging these shuffled series generated a probability distribution of power values at each time–frequency point. For each time–frequency point, raw P values were obtained as percentiles within this distribution (P value resolution of 0.001).

2.3.4. FDR analysis

We corrected the obtained P values for multiple comparisons using the false discovery rate (FDR) method (Benjamini and Hochberg, 1995; Genovese et al., 2002; Ray et al., 2008). This procedure controls for the expected proportion of falsely rejected hypotheses. Using the P values of a given frequency bin, the FDR method was used to find an appropriate significance level below which all time points were considered significant. First, all the P values of the frequency bin (the number of time points was B) were ordered from smallest to largest (denoted by $P(i)$, $i = 1, 2,\ldots,B$). The cut-off level was then given by $P(r)$, where r was the largest i such that

$$P(i) \le i \times \frac{q}{B} \quad (3)$$

where q was the desired FDR (set to 0.05 in this paper). This procedure was repeated for each frequency, yielding a time–frequency map corrected for multiple comparisons in the time domain.

2.3.5. Quantification of high gamma activity

The definition of the high gamma frequency band differed among previous studies. Although the full HGA ranges from 50–150 Hz, only the range from 60 to 120 Hz was used in order to avoid electrical artifacts at 50 and 150 Hz and because this is the frequency range in which the maximal response was obtained. Within this frequency range, we counted the number of frequency bins that displayed significant augmentation at each time point. We termed the resultant number the high gamma broadband index (HGBI). A HGBI of 1.0 or 0 at a given channel indicates all or no bins were significantly increased over whole high gamma frequency band, respectively. A HGBI of 0.5 corresponds to 50% of bins with significant increase.

2.4. Brain normalization

2.4.1. Visualization of spatially normalized channel activity

Anatomical brain images and the positions of the implanted electrode were obtained by preoperative three-dimensional T1-weighted imaging (3D MRI) and 3D CT performed after electrode implantation, respectively. The 3D CT data was then co-registered with the 3D MRI data by maximizing the mutual information between the two datasets. The co-registered 3D-CT was interpolated and re-sliced according to the header information of the 3D-MRI using Dr. View (Asahi Kasei, Tokyo, Japan).

The dataset for the 3D-MRI and the resliced 3D-CT data were imported into SPM8 in ANALYZE format (Welcome Department of Imaging Neuroscience, London, UK; www.fil.ion.ucl.ac.uk/spm). The 3D-MRI of each patient was normalized to the equipped T1-template and converted to Montreal Neurological Institute coordinate space. Each re-sliced 3D-CT dataset was also normalized using the same parameters as were used for the 3D-MRI normalization. After the data conversion, we selected a patient's brain as a repre-

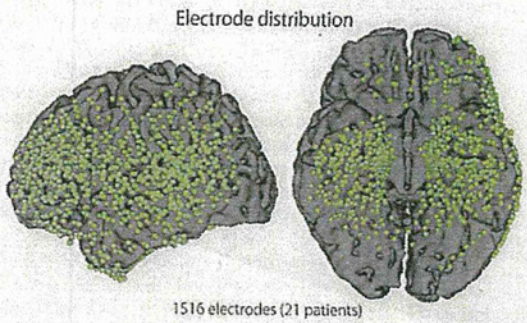

Fig. 1. Electrode distribution. The normalized electrodes were illustrated as green dots in the lateral (left) and basal (right) aspects of the template brain. The electrode positions of each patient were derived from the three-dimensional computed tomography datasets.

sentative brain model and superimposed the electrodes of all patients onto it.

The representative MRI and normalized CT sets of all patients were imported into EMSE (Source Signal Imaging, San Diego, CA) (Ossadtchi et al., 2010). Each electrode location was digitized semi-automatically using predefined electrode templates. EMSE automatically bent the digitized templates to fit the electrodes to the brain surface. Although this procedure carried a risk of registration errors, we compared the results and intraoperative findings during electrode implantation and removal and found that there was little difference between them. We registered the ECoG channels of all patients to the corresponding digitized electrodes (Fig. 1A).

2.4.2. Electrode density correction

To avoid overestimating the HGBI in areas of high electrode density, each HGBI was corrected for the electrode density of the corresponding area by dividing the HGBI by the number of electrodes within 5 mm of each electrode center (cHGBI). cHGBI time series for each channel were displayed on the normalized brain surface using Gaussian interpolation with a sigma value of 10 mm.

2.5. Time series analysis using VOI

We performed volume-of-interest (VOI) analysis to provide quantitative evaluations of HGA dynamics. VOI were assigned to 6 areas that showed representative HGA profiles.

The HGBI of all the electrodes inside each VOI were averaged to show temporal changes. We used a 15 mm VOI radius to prevent overlapping among VOI. For the three language tasks, we used the same set of VOI to enable comparisons among the HGA dynamics of different tasks. If the averaged HGBI in a given VOI corresponded to 1.0, it means all time–frequency bins at all electrodes in the VOI showed a significant increase in high gamma frequency band. The HGBI values in the VOI analysis, therefore, depended not only on the degree of HGA, but also on the number of electrodes which showed strong HGA augmentation.

3. Results

3.1. Summary of the normalized data

The number of patients and electrodes investigated for each task were as follows: the WI task was performed in 21 patients with 1516 electrodes, and the VG and PN tasks were performed in 12 patients with 884 electrodes and 14 patients with 1048 electrodes, respectively. The demographic data of each task group are summarized in Table 1. There was no significant difference between the background data of any group. The normalized electrodes were found to cover an extensive range of the lateral frontotemporal lobes and the basal aspect of the occipitotemporal areas (Fig 1). The distribution of electrodes was similar among the three groups (data not shown).

Table 1
Demographic data of each task group.

	WI	PN	VG	*P* value
No. of patients	21	14	12	
Age	32.4 + −8.95	32.5 + −8.9	32.8 + −9.6	0.99[a]
Sex (M/F)	0.62	0.80	0.50	0.88[b]
Epilepsy onset	17.3 + −10.0	17.6 + −11.0	20.9 + −10.0	0.61[a]
Epilepsy duration	15.0 + −11.4	14.9 + −10.9	11.9 + −9.4	0.70[a]
Epilepsy side (L/R)	1.5	1.8	1.2	0.89[b]
No. of electrodes (base)	33.0 + −6.3	34.9 + −6.1	31.2 + −5.1	0.30[a]
No. of electrodes (Left)	39.2 + −15.1	40.0 + −12.3	42.5 + −17.9	0.83[a]
VIQ	86.8 + −9.6	88.9 + −9.6	87.8 + −9.1	0.81[a]

WI = word interpretation; PN = picture naming; VG = verb generation; VIQ = verbal intelligence quotient.
[a] One-way ANOVA.
[b] Chi-square test.

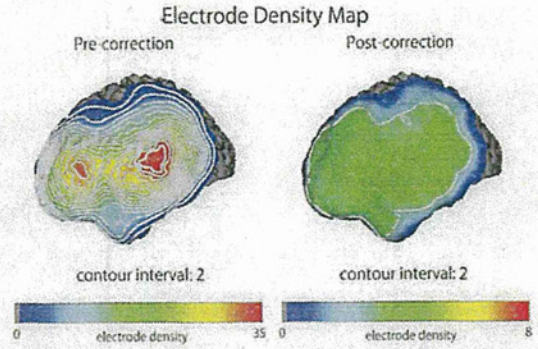

Fig. 2. Electrode density map. Before the correction of electrode density (left), there was high concentration of electrodes in Broca's and Wernicke's areas, reflecting the clinical importance of these areas. The correction resulted in the electrode density becoming almost uniform (right), eliminating the effect of electrode density on the visualization of high gamma activity.

3.2. Electrode density correction

We created electrode density maps to evaluate the heterogeneity of electrode density. Before correction, the electrode density was relatively high in the classical Broca's and Wernicke's areas (Fig. 2A). The correction resulted in the electrode density becoming homogenous throughout the areas covered by the electrodes and was effective at removing the observed electrode density heterogeneity (Fig. 2B).

3.3. Dynamics

We projected cHGBI values onto the brain surface for each language task (Figs. 3–5A).

3.3.1. Spatial distributions of HGA in different tasks

As no electrodes were located in the calcarine fissure, we did not observe the primary responses to the visual stimuli. In the WI task, following the initial recruitment of the bilateral FuG, HGA augmentation in the posterior middle temporal gyrus (pMTG) was observed. In addition, sustained augmentation of HGA was seen over the ventral premotor cortex (vPMC). The latest recruitment occurred over the middle frontal gyrus (MFG) and inferior frontal gyrus (IFG) (Fig. 3A).

Although the dynamics of the PN were similar to those of the WI, the bilateral FuG was more widely involved. Another unique finding was that there was little HGA augmentation in the MFG or IFG during the PN (Fig. 4A).

Since the VG task used auditory stimuli, HGA augmentation was mainly observed in the lateral aspect of the superior temporal gyrus (STG), with no response seen in the basal aspects of bilateral temporal lobes. Subsequently, the pMTG showed HGA augmentation to a similar degree to that seen during the other two tasks. On the other hand, the vPMC displayed slow-onset recruitment. HGA augmentation in the MFG and IFG were maintained until 1000 ms after the VG stimuli, which were similar to those observed during the WI processing (Fig. 5A).